ENSO representation in climate models: from CMIP3 to CMIP5

H. Bellenger[1], E. Guilyardi[1,2], J. Leloup[1], M. Lengaigne[1], J. Vialard[1]

[1] LOCEAN (UMPC-CNRS-IRD-MNHN), IPSL, Paris, France.

[2] NCAS-Climate, University of Reading, United Kingdom.

Submitted to Climate Dynamics

Abstract

We analyze the ability of CMIP3 and CMIP5 coupled ocean-atmosphere general circulation models (CGCMs) to simulate the El Niño Southern Oscillation (ENSO) and the tropical Pacific mean state. The large spread in ENSO amplitude is reduced by a factor of 2 in CMIP5 and the ENSO life cycle (seasonal phase locking, location of surface temperature anomalies) are slightly improved. Other fundamental ENSO characteristics as its spectrum and central Pacific precipitation anomalies however remain poorly represented. Our analyses however reveal that CMIP5 displays an encouraging 30% reduction of the cold bias in the west Pacific. The Bjerknes and shortwave-surface temperature feedbacks, previously identified as major sources of model errors, do not improve in CMIP5. The slightly improved ENSO amplitude therefore might results from error compensations. CMIP3 and CMIP5 can thus be considered as one ensemble (CMIP3+CMIP5). The ability of CMIP models to simulate the observed nonlinearity of the shortwave feedback is assessed. This nonlinearity arises because the real atmosphere switches from subsident (positive feedback) to convective (negative feedback) regimes under the effect of seasonal and interannual variations. Only one third of CMIP3+CMIP5 models reproduce this regime shift, with the remaining models always locked in one of the two regimes. We suggest that an improved mean state results in an improved shortwave feedback non-linearity, and an improved modeled ENSO amplitude. This provides guidance on how to improve the modeled ENSO in CGCMs in a process-based way, avoiding error cancellation. In order to help choosing appropriate models for studying ENSO, we also provide a summary assessment of CMIP3 and CMIP5 models performance in terms of ENSO characteristics and key feedbacks.

1. Introduction

The El Niño-Southern Oscillation (ENSO) is the dominant mode of interannual climate variability. It is characterized by large-scale sea surface temperature (SST) anomalies in the eastern equatorial Pacific Ocean. The amplitude of the SST variations is typically of the order of 1°C and is associated to a change in the oceanic thermal structure and a switch in atmospheric circulation and convective activity. ENSO phenomenon is characterized by an irregular period ranging between 2 to 7 years. A robust feature of the warm ENSO events is the tendency for their peak to preferentially occur in boreal winter, that is, from November to January (Rasmusson and Carpenter 1982). These SST anomalies usually appear and peak in the eastern Pacific, and terminate in the central Pacific. Cold (La Niña) and warm (El Niño) ENSO phase are not symmetrical: SST anomalies are skewed to the positive values.

ENSO basin-scale surface temperature fluctuations induce important changes in the tropical circulation and affects meteorological conditions globally through atmospheric teleconnections (see McPhaden et al 2006 for a review). The most direct effect of ENSO is a seesaw in surface pressure, associated with a modulation of trade winds and a shift of tropical Pacific precipitations. This impacts agriculture, water resources as well as air quality and forest fires in particular in the tropical Pacific neighboring countries (e.g. Naylor et al 2007, Nichol 1997). Knowing whether ENSO characteristics (intensity, frequency…) will change in relation with global warming is a crucial societal need. However, it is not possible to answer this question yet (Vecchi and Wittenberg 2010, Collins et al 2010). It is indeed difficult to model accurately ENSO with Coupled Global Climate Models (CGCMs) because of the complex interplay of various oceanic and atmospheric processes it involves. Understanding, anticipating, and predicting ENSO behavior on seasonal to multi-decadal time scales still poses formidable challenges (Guilyardi et al. 2009a, Wittenberg 2009).

The theoretical understanding of ENSO has significantly increased over the past decades [see Wang and Picaut (2004) for a review]. The oscillatory tendency of ENSO is now fairly well understood. The rise of an El Niño event requires a positive ocean–atmosphere feedback, first described in a seminal paper by Bjerknes (1969), i.e. the tendency of the atmospheric response to central Pacific SST anomalies to further enhance these SST anomalies, is crucial for the growth of ENSO., A number of negative feedbacks have been proposed to explain the termination of warm (El Niño) and cold (La Niña) events, including westward-propagating upwelling Rossby waves reflected at the western boundary into equatorial upwelling Kelvin waves (Suarez and Schopf, 1988), a discharge process due to Sverdrup transport (Jin 1997), western Pacific wind-forced upwelling Kelvin waves (Weisberg and Wang 1997), and anomalous zonal advection of the warm pool (Picaut et al. 1997). The preferential seasonal phase locking of the termination of El Niño warm events during boreal winter have been attributed either to a seasonal modulation of the amplitude of oceanic Kelvin and Rossby waves (Tziperman et al. 1998) or to a southward shift of the El Niño related westerly anomalies in boreal winter (Harrison and Vecchi 1999). The theoretical framework of the recharge oscillator (Jin et al 2006) provides an example of a synthetic view of ENSO fundamental processes. It shows how coupled air-sea processes can either promote a thermal damping (through the negative feedback of surface heat fluxes, but also the mean advection and upwelling), or a growth of SST anomalies. The latter results from positive SST anomalies that develop as the response of zonal advection, Ekman pumping and thermocline depth anomalies to large scale wind anomalies.

Despite progresses in understanding and simulating basic ENSO features, CGCMs from the third Coupled Models Intercomparison Project (CMIP3) were still struggling with its simulation. The CMIP3 database in particular displays a large diversity of ENSO amplitude (van Oldenborgh et al 2005, Guilyardi 2006, Yu and Kim 2010), a tendency to produce a regular biennal oscillation rather than a broad spectral peak in the 3-8 year band, a poorly represented seasonal phase locking (AchutaRao and Sperber 2006, Guilyardi et al 2009a) and variability that extends too far into the western Pacific (Leloup et al. 2008, Yu and Kim 2010). The CMIP3 models also have limited skills in simulating the long-term mean and annual cycle in the tropical Pacific Ocean. This has been pointed out as a probable origin for part of the diagnosed biases in the modeled ENSO (van Oldenborgh et al 2005, Guilyardi 2006). The biases in ENSO characteristics are also associated with issues in representing the individual ENSO mechanisms (van Oldenborgh et al 2005, Kim and Jin 2011): for instance, van Oldenborgh et al (2005) showed that most CMIP3 models have a too weak wind response to SST anomalies. This impacts thermocline variability, zonal advection and thermal damping with the possibility of error cancellations (Kim and Jin 2010).

Several CGCM analyses point out the central role of the atmospheric component in shaping the modeled ENSO (Guilyardi et al 2004, Capotondi et al. 2006, Lengaigne et al 2006, Toniazzo et al 2008, Kim et al. 2008, Guilyardi al. 2009b, Watanabe et al. 2010, Lloyd et al. 2011), with a special emphasis on convective processes (Neale et al. 2008 Wittenberg et al 2003, Wu et al 2007, Guilyardi et al 2009a, Lengaigne and Vecchi 2010, Watanabe et al 2011). The main atmospheric processes driving ENSO evolution are usually described simply as two linear feedbacks (see Jin et al 2006): (i) the dynamical Bjerknes feedback (μ , Bjerknes 1969) and (ii) the heat flux feedback (α , Zebiak and Cane 1987). The Bjerknes feedback μ is defined as the coupling coefficient between equatorial SST anomalies (within the 160°E-150°W, 5°N-5°S region, also known as Niño-3) and the remote zonal wind stress response (within the 150°W-90°W, 5°N-5°S region, also known as Niño-4). μ is a measure of the positive retroaction that gives rise to ENSO. The heat flux feedback, α, is measured as the coupling coefficient between surface heat fluxes (within the Niño-3 region) and SST anomalies in the same region. It is usually a negative feedback that can be broken into four components (Lloyd et al 2009, 2011 and 2012), dominated by the shortwave (α_{SW}) and latent feedbacks (α_{LH}).

As pointed out by Zebiak and Cane (1987) and Barnett et al. (1991) a linear shortwave feedback is a crude approximation of the complex cloud processes involved in ENSO. The shortwave feedback is indeed quite different depending on the stability of the atmosphere. In unstable situations, a higher SST leads to an increase in convection, high clouds, and a decrease in surface shortwave flux: the shortwave feedback (α_{SW}) is negative in the convective regime. Under stable conditions, a higher SST destabilizes the atmospheric boundary layer and prevents the formation of stratiform boundary layer clouds (Philander et al 1996, Xie 2005). This leads to an increase in shortwave flux at the surface: α_{SW} is a positive feedback in the subsident regime. In nature, the shortwave feedback indeed tends to be negative for warm SST anomalies and positive for cold SST anomalies. Lloyd et al. (2012) discuss the nonlinearity of the shortwave feedback in CMIP3 climate models and stress its importance for correctly modeling ENSO.

In line with the approach proposed by Gleckler et al (2008) to characterize model performances, a CLIVAR Pacific Panel working group has proposed a set of standard metrics for ENSO (Guilyardi et al 2009b). These metrics describe both ENSO variability (in terms of SST and precipitation anomalies in selected regions) and the background tropical Pacific mean state. This set of metrics can usefully be complemented by the analysis of Bjerknes and heat flux feedbacks, that give more insights on whether ENSO is correctly simulated for the right reasons (e.g. Lloyd et al 2009).

In this paper, we present an assessment of basic ENSO properties and associated feedbacks in CMIP5 control simulations, and a comparison with CMIP3. Section 2 presents the datasets and metrics used to assess ENSO in CMIP models. A synthetic view of ENSO simulation in CMIP5 models and of the main changes with respect to CMIP3 is provided in section 3. Section 4 addresses the representation of atmospheric feedbacks in the models. Our analysis of process-based metrics shows that the heat flux feedback, and in particular its shortwave component, remains a large source of uncertainties in CMIP3 and 5 models. Building on Lloyd et al (2012), we explore the shortwave feedback, its nonlinearity and its potential implications on simulated ENSO characteristics in more details in Section 5. Section 6 presents a synthesis of ENSO and of the main atmospheric feedbacks representation in each model. Section 7 provides a summary and discussion.

2. Datasets and methods

The Coupled Models Intercomparison Project aims at coordinating climate change experiments. CMIP3 experiments provided basic material for scientific studies used in the Intergovernmental Panel on Climate Change (IPCC) Fourth Assessment Report (AR4, Meehl et al 2007), while CMIP5 have been designed to prepare the AR5 (Taylor et al 2012). We use multi-century pre-industrial simulations for the entire CMIP3 ensemble (24 models) and for 33 available models from CMIP5. Simulation are at least 100 years-long but more than half of them (32 out of 57) are 500 years or longer (Table 1) as required to ensure statistical robustness for the computation of ENSO spectra (Wittenberg 2009, Stevenson et al. 2010). We use monthly-averages outputs on the atmospheric grid for SST, zonal surface wind stress, surface precipitation and the net heat flux and its components (radiative and turbulent heat fluxes). Monthly anomalies are computed by subtracting the experiment-average seasonal cycle. Metrics for each climate model are compared against similar measures derived from observations. We use the HadISST1.1 1900-1999 Sea Surface Temperature (SST) from Rayner et al. (2003) for determining the spectrum of SST anomalies timeseries, ERA40 SST and zonal surface wind stress (Uppala et al. 2005), CMAP precipitation (Xie and Arkin 1997) and OAFlux surface fluxes (Yu and Weller 2007).

We use the metrics developed within the CLIVAR Pacific Panel, which assess the tropical Pacific mean state and interannual variability. The four ENSO metrics encompass ENSO amplitude (Niño-3 SST standard deviation), structure (Niño-3 and Niño-4 amplitudes), frequency (RMSE of Niño-3 SSTA spectra) and heating source (Niño-4 precipitation standard deviation). Two additional metrics are defined in this study: a measure of the amplitude of the ENSO biennial component (the ratio of the Niño-3 SST anomaly timeseries power in the 3-8 years and 1-3 years bands) and measure of the seasonality of ENSO (ratio between winter November-January over spring March-May average Niño-3 SST anomalies standard deviations). The other metrics are defined as the RMSE of annual average simulated mean state against the observed one diagnosed using SST, zonal wind stress, precipitation and surface heat flux. The last metric evaluates the simulated annual cycle of SST in Niño-3 (Guilyardi and Wittenberg 2010).

An additional diagnosis allows to assess the spatial characteristics of ENSO events in CMIP3/CMIP5 ensembles. El Niño and La Niña events are defined as in Leloup et al. (2008) using the mean SST anomalies along the equatorial Pacific (150^{o}E-90^{o}W, 5^{o}S-5^{o}N). For each model, we compute a threshold t corresponding to half of the standard deviation of this time series. We define El Niño (resp. La Niña) as any period for which mean equatorial Pacific SST anomalies are greater (resp. lower) than t (resp. minuq t) during at least six consecutive months. The onset, peak and termination of an El Niño (La Niña) event are then defined as respectively the beginning, maximum (minimum) and end of the period above the threshold. For each of those phases (onset, peak and termination), the position of the maximum (minimum) along the equatorial region is located, dividing the equatorial Pacific in three main regions: West (150^{o}E-170^{o}W, 5^{o}S-5^{o}N), Central (170^{o}W-130^{o}W, 5^{o}S-5^{o}N), and East (130^{o}W-90^{o}W, 5^{o}S-5^{o}N).

The atmosphere process-based metrics are computed following Lloyd et al (2009, 2012). The Bjerknes feedback μ is computed as the linear regression coefficient between Niño-4 average zonal surface wind stress monthly anomaly τ_x' and Niño-3 average SST monthly anomaly SST', that is $<\tau_x'>_{\text{Niño-4}} = \mu <SST'>_{\text{Niño-3}}$ where $<\ldots>_{\text{Niño-3}}$ means spatial average over Niño-3 region. Whereas the Bjerknes feedback is a non local large-scale response to a large-scale SST anomaly, the heat flux feedback is a local response to local SST variations. The net heat flux feedback α is thus computed as the spatial average over Niño-3 of the point-wise regression coefficient of the net heat flux monthly anomaly Q' and SST', that is $\alpha =< \alpha_r >_{\text{Niño-3}}$ where α_r satisfies $Q'(r)= \alpha_r SST'(r)$ for each region r in Niño-3. The four components of α are computed in the same way by replacing Q' by the considered component (sensible and latent heat fluxes and shortwave and longwave fluxes).

3. ENSO in coupled models : from CMIP3 to CMIP5

We present a synthetic view of how ENSO is modeled usingthe CLIVAR Pacific Panel metrics (Guilyardi et al 2009b). These metrics can be divided into two groups: those characterizing ENSO variability and those characterizing the climate mean state in which this variability occurs. Figure 1 sums up ENSO characteristics for CMIP3 and CMIP5 models in comparison to observations. Even though we discuss the main multi-model features, the figure shows the metrics for all centers and models.

Figures 1a and b show that the average of modeled ENSO amplitude in CMIP5 (red squares) and CMIP3 is comparable to observations in both Niño-3 and 4. However, the range of CMIP5 ENSO amplitude spread around the observed value is reduced by about half compared to CMIP3 in the two regions (whiskers). This is a clear improvement over the CMIP3 ensemble where ENSO amplitude diversity was larger than could be explained by observational variability (e.g. Guilyardi et al 2009a). Indeed, 65% of CMIP5 Niño-3 and Niño-4 ENSO amplitudes fall within 25% of the observed value against 50% for CMIP3.

One of the most important features of ENSO in terms of climate impacts and teleconnections is its impact on atmospheric convection and hence on precipitation and large-scale circulation (e.g. McPhaden et al 2006). This is evaluated here using the standard deviation of Niño-4 precipitation anomalies (Fig. 1c). Most models tend to underestimate ENSO-related interannual anomalies of the convective activity in the central Pacific. There is no clear improvement of the average value of the metric in CMIP5 compared to CMIP3 (~40% of ENSO-related convective activity falls within 25% of the observed value for both CMIP3 and CMIP5).

The 2-7 year timescale is a key property of ENSO variability that is difficult to correctly represent in climate models. In order to evaluate the ability of a model to simulate correctly ENSO timescale, we compute here the RMS difference (in °C^2) of simulated and observed Niño-3 SST monthly anomaly spectra. This spectral metric (Fig. 1d) hardly shows any change from CMIP3 to CMIP5. Figure 2a shows the Niño-3 SST anomaly spectra for the reference and two examples from CMIP3 and CMIP5. This illustrates the tendency for some models to represent ENSO with a too short period of about 2 years (MIUB and BCCCSM1.1) or having a spectral peak for longer periods (between 3-8 years like CSIROmk35 and MIROC5). Therefore, the ENSO spectra characteristics are further studied by computing the ratio between the energy in the 1-3 years band and the one in 3-8 years band (Fig. 2b). The observations show a ratio of 1.2 (i.e. slightly more spectral power in the lower frequency range). Both ensemble show a large diversity among the models: some models have twice as much energy in the 1-3 years band than in the 3-8 years band, for some others this ratio is inverted. According to this analysis, some improvement can be seen from CMIP3 to CMIP5: 25% of CMIP3 models against 40% of CMIP5 models exhibit a ratio within 25% of the observed one. Note that Wittenberg (2009) and Stevenson et al. (2010) show that a minimum of 300 to 500 years is necessary to accurately evaluate the ENSO spectrum. As reliable observational records are still quite short, even the real ENSO spectrum remains uncertain.

ENSO variability is characterized by a strong phase locking to the seasonal cycle with maximum of SST anomaly in November-January and a minimum in March-May (Fig. 3a). This ENSO phase locking is particularly important for ENSO teleconnections and for instance for the link between El Niño and the Indian summer monsoon (e.g. Webster et al 1998). On average, both CMIP3 and CMIP5 ensemble show a comparable though weaker than observed seasonal phase locking (Fig. 3a). Of course, individual models show a variety of behavior with ENSO peaks during any season. In both ensembles 50% of the models show a peak in November-January. Figure 3b shows the seasonality metric defined as the ratio of SST anomaly seasonal cycle between November-January and March-May. This metric synthetizes both seasonal amplitude and phase of the modeled ENSO signal. There is 55% of CMIP5 models against 40% of CMIP3 models that have ENSO seasonality metric within 25% of the observed one. In particular some models from CMIP5 ensemble show a seasonality that is very close to the observed one (BCC-CSM1, CanESM2, GFSL-ESM2G, GISS and FGOALS models, MIROC4h, NCC and CESM1 models, see Fig. 3b). So ENSO seasonal phase locking is slightly improved from CMIP3 to CMIP5.

The surface warming (cooling) pattern associated to an El Niño (La Niña) event evolves during its life cycle, and impacts ENSO teleconnections (e.g. Webster et al 1998). Figure 4 shows the position of the maximum SST anomaly for each phase (onset, peak, termination) for the observations, CMIP3 and CMIP5. For El Niño onset (Fig. 4a), CMIP3 and CMIP5 models ensemble mean both underestimate the percentage of onsets with a maximum in the Eastern Pacific (65% vs. 80% in observations) while they tend to overestimate onsets with a maximum in the Central and West Pacific. CMIP5 models on average correctly simulate 75% of La Niña onsets in the eastern Pacific (Fig. 4d), an improvement with respect to CMIP3 (only 65%). Both CMIP ensembles tend to underestimate the observed number of El Niño (~80%) and La Niña (~90%) peaks in the central Pacific, with a slight improvement in CMIP5 (an average of 60% El Niño events peaking in the eastern pacific compared to 45% in CMIP3). Both CMIP ensembles tend to produce unrealistic ENSO terminations in the western Pacific, and less terminations than observed in the central Pacific (Figures 4c and 4f), with some improvement in CMIP5 against CMIP3. Figure 4g provides a more detailed view of the percentage of central Pacific El Niño peaks in individual models. Some models simulate only 10% of El Niño events with a maximum in the eastern Pacific while others reach values close to 100%.

Simulated and observed ENSO characteristics may depend on the mean state in the tropical Pacific Ocean (e.g. Wang and An 2002, Guilyardi 2006, Sun et al 2009). Here we discuss tropical Pacific background biases relevant to ENSO variability in CMIP3 and CMIP5. The multi-model ensemble-average mean state metrics (Fig. 5) only show small changes from CMIP3 to CMIP5. There is a deterioration of the simulation of the east Pacific average net surface flux (Fig. 5e) with an average error exceeding $40 Wm^{-2}$ for Niño-3 region. Other CMIP5 mean state metrics show slight if any improvement compared to CMIP3 and the mean errors remain large. The SST mean state in the tropical Pacific ocean exhibits errors of about 1.5°C on the average for both ensembles (Fig. 5a), the mean zonal wind stress at the Equator in the Pacific shows errors of about $1.5\ 10^{-2}\ N.m^{-2}$ (Fig 5c), and the average precipitation in the Indo-Pacific region shows RMSE of roughly $2\ mm.day^{-1}$ (Fig. 5d). There is however a bit more convergence amongst models in CMIP5 (slightly smaller spread in Tropical Pacific SST, precipitation and wind stress rms-error, and nino3 SST seasonal cycle than in CMIP3). The SST seasonal amplitude in Niño-3 has for example less extreme values in CMIP5 than in CMIP3 (Fig. 5b; 60% of CMIP5 models have values within 25% of the observed one against 45% only for CMIP3).

The zonal structure of the coupled system at the equator determines the interaction between ENSO and the mean state (Wang and Picaut 2004). To gain insights on the simulated mean state in CMIP3 and CMIP5, we show the average SST and zonal surface wind stress at the equator on Figure 6. The 1°C cold bias in the western equatorial Pacific is reduced by roughly one third in CMIP5, but it remains unchanged in the east (Fig. 6a). The warm bias in the far eastern Pacific (east of 260°E) remains similar in the two ensembles. There is however a better representation of the zonal SST gradient in CMIP5 (Fig. 6a), with a corresponding improvement of the average zonal wind stress in the central Pacific (Fig. 6b). Around 140°W, the bias in CMIP3 is reduced by roughly 40% in CMIP5 giving a better zonal wind stress gradient along the equator. Yet, both CMIP3 and CMIP5 exhibit an easterly stress bias west of the dateline.

4. Atmosphere process-based metrics

The analysis of Kim and Jin (2011) suggests that both the heat flux and Bjerknes feedbacks contribute to CMIP3 model errors. It is thus interesting to investigate if there is any progress in the representation of those feedbacks in the CMIP5 ensemble.

As shown on Fig. 7a, there is no qualitative change in the multi-model ensemble average Bjerknes feedback μ. On average, μ is similar for CMIP3 and CMIP5, with most models underestimating the amplitude of this positive feedback by 20 to 50%. Only 20% of CMIP3 and CMIP5 models fall within 25% of the observed value ($12\ 10^{-3}\ Nm^{-2}/C$) of the Bjerknes feedback. The observed heat flux feedback α ($-18\ Wm^{-2}/C$, Fig. 7b), is similarly underestimated by most CMIP3 and CMIP5 models. There is a large spread among models and only 10% of CMIP3 and CMIP5 models fall within 25% of the observed value.

To gain insights on the reason for such a large spread in modeled α, we investigate its two major components: the shortwave and the latent heat flux feedbacks (Lloyd et al 2012, Figure 7c and d). Despite a degradation of the background mean state net heat fluxes in Niño-3 (Fig. 5e), α does not show a corresponding evolution between CMIP3 and CMIP5 (Fig. 7b). In addition, the latent heat flux feedback is on average improved in CMIP5: although most models still underestimate the amplitude of this negative feedback, more CMIP5 models (50%) fall within 25% of the observed α_{LH} than in CMIP3 (one third).

CMIP3 and CMIP5 ensembles both poorly reproduce the observed shortwave feedback value of -7 $Wm^{-2}K^{-1}$, with ensemble average values of α_{sw} close to zero. (Fig. 7c). The diversity in simulated α (standard deviation of about $4Wm^{-2}/C$ for both CMIP3 and CMIP5) is clearly due to the large diversity of α_{SW} in both ensembles (standard deviation of about $5Wm^{-2}/C$ for both CMIP3 and CMIP5), as already shown by Lloyd et al (2012) using CMIP3. In the CMIP5 ensemble, there are broadly two distinct groups of models: those producing a positive α_{SW}, and those producing a negative α_{SW} as observed. Only 10% (3) of CMIP5 models display a α_{SW} value within 25% of the observed one, against 5% (one model) for CMIP3. CMIP5 models still struggle to represent convection and cloud processes (e.g. Jiang et al 2012). Yet, these processes are critical for the simulation of the shortwave feedback as showed by Lloyd et al (2011, 2012).

5. Nonlinearity in atmospheric SW flux feedback

As demonstrated in the previous section, the diversity in shortwave feedback is the major contributor to the diversity in heat flux feedback, and hence propably a major contributor to errors in the simulated ENSO (Kim and Jin, 2011). In particular, this feedback is actually not linear (Zebiak and Cane 1987, Barnett et al 1991). The shortwave feedback (α_{SW}) is indeed negative for warm SST anomalies (El Niño conditions) and positive for cold SST anomalies (La Niña conditions). Lloyd et al. (2012) depict the nonlinearity of shortwave feedback in CMIP3 models and stress the importance of its representation for a proper representation of ENSO. This section aims at gaining further insights on this particular issue. The changes between CMIP3 and CMIP5 regarding ENSO variability and the process-based metrics results (figures 1 to 7) are relatively modest. We hence group all model simulations into a larger ensemble, and distinguish members within this ensemble depending on the ability of each model to represent the shortwave feedback nonlinearity.

Lloyd et al. (2012) estimates α_{SW} nonlinearity from the difference α_{SW}^{-}- α_{SW}^{+} of the linear regression coefficient of shortwave flux anomaly computed separately for positive (α_{SW}^{+}) and negative (α_{SW}^{-}) SST anomalies in the Niño-3 region. This approach is justified from the scatterplots of observed shortwave against SST anomalies (fig. 8b in green) which displays a roughly linear behavior by segment with a breakpoint roughly around 0°C. More advanced methods of segmented linear regression, with a breakpoint determined iteratively for each particular model, were applied without qualitative changes in the conclusions. We thus stick to the Lloyd et al. (2012) method for the sake of simplicity and consistency with this previous study.

Figure 8a-c shows examples of monthly shortwave against SST anomalies in Niño-3 for three selected models. Some models display an α_{SW} which is always positive (Fig. 8a) or negative (fig. 8c), irrespective of the sign of SST anomalies, i.e. with weak nonlinearity in the Niño-3 shortwave feedback. These two types of models are characterized by a single atmospheric regime-like behavior in eastern equatorial Pacific that is either mainly subsiding (the SUB type corresponding to an always positive α_{SW}, 23 models, fig. 8d, and Table 1) or mainly convective (the CONV type corresponding to an always negative α_{SW}, 12 models, fig. 8f). The 21 remaining models (the MIX type, Fig 8b and e) display a comparable behavior to observations with a shift from positive α_{SW}^{-} (subsident condition) for negative SSTA in Niño3 to a negative α_{SW}^{+} (convective conditions) for positive SSTA in Niño3. Table 1 provides the regime (MIX, CONV or SUB) of each model analysed in this study. Figure 8e shows that some models manage to reproduce α_{SW}^{-} (La Niña conditions) or α_{SW}^{+} (El Niño conditions) with the correct order of magnitude.

Figure 9 shows that the amplitude of ENSO-related SST variation and the nonlinearity in α_{SW} are strongly related with a positive linear correlation coefficient of 0.71 (significant at 99%). By construction, models with large α_{SW} nonlinearity are characterized by a MIX-type α_{SW} with a change of regime from subsiding to convective for SST<0 and >0 respectively. These models also show the largest ENSO amplitude. Interestingly, MIX-type models also have the strongest precipitation response to ENSO in Niño-4 (Table 2) followed by CONV-type models, and SUB-type models showing the weakest value. One likely reason for strongest ENSO amplitude in MIX-type models is that strong SST interannual variations are responsible for the nonlinearity in α_{SW}. In other words, strong SST variations are necessary to switch the atmospheric regime between SUB and CONV in Niño3. On the other hand, the change in atmospheric regime on the ENSO amplitude certainly impacts on the simulated atmospheric feedbacks: When α_{SW} nonlinearity is weak, α_{SW} has always the same sign, positive for SUB-type and negative for CONV-type (Fig. 8d and f). Taking only α_{SW} into account, this would mean amplified SST variations for SUB-type and damped for CONV-type with MIX-type models lying in-between. However, α_{SW} is not the only feedback that depends strongly on the atmospheric regime. The Bjerknes feedback depends on the SST anomaly but also on elevated convective heating associated to convection over Niño-3 according to the Gill model (Gill 1980, Chiang et al 2001). Simulated Niño-3 average precipitation and Bjerknes feedback are indeed linearly correlated at 0.55 among CMIP3+CMIP5 models (significant at 99%). This explains why SUB-type models tend to have a weaker average Bjerknes feedback than CONV-type models (Table 2) with again MIX-type models lying in-between. It is however not possible to interpret further the impact of these changes in feedbacks on ENSO amplitude. This would certainly require an additional analysis of the oceanic response to these atmospheric feedbacks that is beyond the scope of this study. At this point, the link between the nonlinearity in shortwave feedbacks and ENSO amplitude remains thus an open question.

Lloyd et al (2012) suggested that nonlinearity of shortwave feedback might play a role in ENSO skewness, by being positive in La Niña conditions and negative in El Niño. We did not find any clear link between α_{SW} nonlinearity and Niño-3 SST anomaly asymmetry (linear correlation coefficient of 0.2). Yet, stratifying the multi-model database by their regime types (Fig. 10a), it is clear that the seasonal variations of α_{SW} differs from one type to another: Whereas SUB types models show a constant positive shortwave feedback throughout the year, CONV and MIX types models show a clear decrease of α_{SW} during winter and spring. This seasonal increase in the α_{SW} ENSO damping term corresponds to the warmest SST and the associate increase in convective activity in eastern Pacific that is also observed. The spring minimum in ENSO amplitude (Fig. 3b) corresponds to this largest negative α_{SW} feedback (i.e. triggering of convection) in observation. Although weaker, this is also the case for MIX and CONV-type models (fig. 10a). The simulated increase of the negative shortwave feedback may thus contribute to damp SST anomalies during spring, and hence contribute to the phase locking of ENSO amplitude for MIX and CONV models. Figure 10b shows the scatterplot of the ENSO seasonal metric (fig3b) against the average value of α_{SW} in March-April-May. In spite of the large spread, there is indeed a clear link between the ability of the model to have a strong shortwave damping in spring and its ability to reproduce a clear seasonal ENSO phase locking (linear correlation coefficient of -0.51, significant to the 99% level). Table 2 summarizes the average ENSO seasonal metric and the March-April-May average α_{SW} for the different types of models. MIX and CONV types model tends to have an ENSO seasonal metric closer to the observed (1.45) associated with a negative α_{SW} during spring. This suggests that a model has to be able to reproduce the seasonal switch to the convective regime in order to represent this fundamental characteristic of ENSO.

We now explore the link between the ability of the models to represent the different regime in the eastern Pacific and their simulated mean state. Figure 11 represents the average equatorial Pacific mean state in SST and zonal wind stress for SUB, MIX and CONV-type models (to be compared to Fig. 6). On average, CONV-type models are the warmest with comparable negative bias in the western Pacific Ocean (of about 0.5°C) but the strongest positive one in the east (up to 1°C, Fig. 11a). This warm bias in the east may partly explain the fact that these models are characterized by convective regime in Niño-3. SUB-types models show a cold bias over all longitudes west of 260°E, coherent with enhanced trade winds over the Pacific Ocean, and thus a stronger Walker circulation. MIX-type models are comparable to CONV-type models in the western Pacific and to SUB-type in the east. In particular, the zonal SST gradient is stronger and closer to the observed one for MIX-type models. The difference in equatorial zonal wind stress between the different types of models is less clear (Fig. 11b), especially in the Central Pacific. MIX-type models however display an equatorial zonal wind stress mean state that is closer to observations. Figure 12 shows the link between the equatorial zonal SST gradient / mean biases and the nonlinearity of the shortwave feedback. Linear correlation coefficients are relatively low (c=0.25 is not significant at the 95% level) but Spearman rank correlations are both significant at the 99% level. This implies that a mean state close to the observations, i.e weaker mean bias and better SST zonal gradient, will enable strong nonlinearities in the shortwave feedback, i.e. switches from subsident to convective regime in the eastern Pacific Ocean, which are associated to an improved ENSO amplitude simulation (figure 9).

6. ENSO and atmospheric feedbacks scores

This section provides a synthesis of each CMIP3 and CMIP5 model performances in terms of ENSO. In order to characterize how models represent basic features of ENSO, a sub-set of four metrics are selected: the Niño-3 SST anomaly variability (fig. 1a) to depict the simulated ENSO amplitude; the percentage of El Niño events peaking in the eastern Pacific (fig. 4g) to qualify ENSO spatial structure; the ratio of power within the 3-8 year and 1-3 year bands (fig. 2b) to describe the ENSO spectrum; and the ratio between Niño-3 SST anomaly standard deviation in November-January and March-May (fig. 3b) to represent ENSO seasonal phase locking. For each metric *m* and each model *i*, we compute e_i, the absolute value of the error compared to observations (*ref*) that is normalized by the CMIP3+CMIP5 intermodel standard deviation ($\sigma_{CMIP3+CMIP5}$) following:

$$e_i = \frac{\left| m_i - m_{ref} \right|}{\sigma_{CMIP3+CMIP5}} \qquad (1)$$

An overall ENSO score is then define as the average of these normalized errors, the lower the ENSO score, the better the model represents the basic characteristics of ENSO on the average. Because models can however correctly simulate ENSO with erroneous physical feedbacks (e.g. Guilyardi et al 2004), we also use the four processed-based metrics presented in this study (Fig. 7) in order to evaluate the fidelity of simulated atmospheric feedbacks. The normalized errors of μ, α, α_{SW} and α_{LH} are computed following (1) and their average defines a "Feedback score" for each model in the same fashion as for the "ENSO score". The normalized errors for each selected metric and the ENSO and Feedback scores are reported on Figure 13. Note that lower scores values correspond to better skill in representing ENSO and its atmospheric feedbacks.

The average ENSO score for CMIP5 models is 0.87 (std. dev. 0.34). This shows some improvement compared to the 1.27 (std. dev. 0.47) average score for CMIP3. In contrast, the average Feedback score of CMIP5 is 1.66 (std. dev. 0.62) and is close to the average score of CMIP3 ensemble that is 1.84 (std. dev. 0.62). This indicates that fundamental air-sea interactions responsible for ENSO amplitude are still poorly represented in CMIP5. 25% (8) of CMIP5 models however have a Feedback score inferior to 1 compared to less than 10% (2 models) for CMIP3.

Figure 14 shows the scatterplot of the ENSO score as a function of the Feedback score for all models. There is no clear correlation (linear correlation coefficient of 0.03) between the two scores. Some models such as MIUB (CMIP3, 16_c3 on fig. 14) have relatively good atmospheric feedbacks (Feedback score lower than 1) but somehow the modeled ENSO characteristics are not accurate (large ENSO score of 2.3). On the contrary, GFDL-ESM2G, HadGEM2s, MPI-ESMs, and NCCs (CMIP5, respectively 9b, 17 a and b, 18a and c and 21a and b on fig. 14) show relatively good ENSO characteristics (ENSO score lower than 1) despite an improper representation of the feedbacks with Feedback score of 1.5 and higher (Fig. 14). This certainly reflects the importance of oceanic feedbacks for ENSO, but it can also be the sign of the interplay of compensating errors.

Taking advantage of the large CMIP3+CMIP5 ensemble, we have been able to distinguish the models considering their ability to simulate changes in the atmospheric regime in the eastern Pacific Ocean. Colors on Figure 14 refer to the type (SUB in blue, MIX in black and CONV in red) of the model. For these three categories, the average ENSO score is comparable (around 1.05 with standard deviations of about 0.5). One can however note, that among the models with the best ENSO score (of less than 0.5), two are of MIX (NorESMs) and CONV types (FGOALSg2) and one of the SUB type. The average Feedback scores are clearly better for CONV (1.15, std. dev. of 0.47) and MIX (1.63, std. dev. of 0.54) than for

SUB (2.15, std. dev. 0.44) as a result of better representation of the Bjerknes feedback (stronger μ on the average, see Table 2) and of the negative shortwave feedback whereas SUB tends to produce a positive shortwave feedback (fig. 8).

It would be tempting to define a ranking of models from this analysis and rule out models for ENSO studies. However, these scores are based on a sub-set of metrics with no particular hierarchy between them. The results displayed in figures 13 and 14 may thus be seen as a proposition for the use of the synthetic information contained in metrics and not as a precise and definitive ranking of the models. Both the choice of the metrics and the method to compute the scores can be revisited according to one's specific interest. Here we are interested in particular in characterizing the ability of the model to correctly simulate the basic features of ENSO together with the atmospheric feedbacks. In this context, these scores remain interesting to compare groups of models and in particular to detect the evolution from CMIP3 to CMIP5. The CMIP5 FGOALSg2, GISS2E models, CESM1-FASTCHEM, MIROC4h, CNRM-CM5, GFDL-ESM2-M, CCSM4 models and the CMIP3 CCCMAt63 model all have both ENSO and Feedback scores below 0.4. These models, that are all of the CONV or MIX-type, may thus be more appropriate to study ENSO mechanisms.

7. Conclusion and discussion

7.1 Summary

The CMIP5 multi-model ensemble does not exhibit a quantum leap in ENSO performance compared to CMIP3. The ENSO amplitude however exhibits less diversity in CMIP5 than in CMIP3: 65% of CMIP5 models ENSO amplitude falls within 25% of the observed value against 50% for CMIP3. The ENSO life-cycle is also slightly improved in CMIP5. There are in particular improvements in ENSO seasonal phase locking (fig. 3b) and in the location of the strongest SST anomalies during the onset and peak phases of El Niño and La Niña (fig. 4). ENSO termination however tends to occur much more to the west than in observations in both CMIP3 and CMIP5. The multi-model mean state ensemble average does not change radically between CMIP3 and CMIP5 either. There are however some improvements in the simulation of the mean SST and zonal wind stress in the equatorial Pacific (Fig. 6) in CMIP5, associated with a reduction of the CMIP3 cold bias in the Western Pacific by 30 to 40 %. This modest improvement in the simulated mean state may explain the slight improvement in ENSO characteristics although it is difficult to conclude firmly on that topic. Only a few models score better for all metrics and most have pluses and minuses.

We also evaluated simple metrics of the atmospheric feedbacks (Bjerknes and heat flux feedbacks) that are thought to play a major role in ENSO physics (Guilyardi et al 2009). Examination of these important physical feedbacks (Kim and Jin 2011) shows no clear improvement in a multi-model sense, although some models do improve. This highlights that there is still potential for error cancellation in CMIP5 models. In other words, the convergence of ENSO amplitude in CMIP5 may not be grounded on physical processes. Most CMIP5 models still underestimate the observed positive Bjerknes feedback (on average by roughly 30%). Finally, comparing CMIP3 and CMIP5 reveals that, whereas the latent heat flux feedback is improved due to its close relationship with SST variations (Lloyd et al. 2011), the shortwave feedback remains a dominant source of errors. The convergence of the simulated interannual SST variability from CMIP3 to CMIP5 might thus be the sign that ENSO basic features are now taken into account when tuning the models, rather than a real improvement of important air-sea feedbacks for ENSO.

Nonlinearity in feedbacks is usually not taken into account in theoretical approaches of ENSO representation in CGCMs (e.g. Jin et al 2006). The very diversely simulated shortwave feedback is characterized by a strong nonlinearity in observations: the shortwave feedback is generally negative for positive SST anomalies (convective regime) and positive for negative SST anomalies (subsident regime). Most models are however perpetually locked in one of these regimes in the eastern equatorial Pacific. Only a third of the CMIP models can reproduce the observed regime shift and the change in α_{SW} sign. There is a strong relationship between the modeled shortwave feedback nonlinearity and the ENSO amplitude. The models with the stronger nonlinearity in α_{SW} are also the ones with stronger ENSO. It is possible that a larger variability of SST in Niño-3 favors the shift in atmospheric regime, but a large ENSO amplitude may as well be a consequence of this ability to switch from convective to subsident regime. Surprisingly, there is no strong evidence of a link between the α_{SW} nonlinearity and ENSO asymmetry. However, the ability to switch to convective regime seasonally seems to be linked with the damping of SST anomalies in spring and thus with ENSO phase locking.

Using the synthetic information encapsulated in a few simple ENSO performance metrics together with atmospheric feedbacks process-based metrics, it is possible to indicate models that produce a correct ENSO signal with a reasonable representation of underlying processes. This approach suggests that the FGOALSg2, GISS2E, CESM1-FASTCHEM, MIROC4h, CNRM-CM5, GFDL-ESM2-M, CCSM4 models from CMIP5 and CCCMAt63 model from CMIP3 have both the best ENSO characteristics and the best atmospheric feedbacks. These models may be more reliable to study ENSO dynamics, and its sensitivity to external forcing.

7.2 Discussion and perspectives

Much development work for modeling group is still needed in order to correctly represent ENSO, its basic characteristics (amplitude, evolution, timescale, seasonal phaselock…) and fundamental processes such as the Bjerknes and surface fluxes feedbacks. The Bjerknes feedback is still strongly underestimated by most models. Marti et al (2010) suggested that the atmospheric horizontal resolution may have an impact in simulating the

Bjerknes feedback, but this still needs to be fully addressed. Furthermore, the zonal wind stress over Niño-4 is also sensitive to Niño-3 convective activity through Gill-type response (Gill 1980) and is thus sensitive to the AGCM convective scheme (e.g. Watanabe et al 2011). This provides interesting leads to work on the improvement of this fundamental ENSO process.

The damping surface flux feedback also remains too diverse in CMIP5 models, in particular due to the difficulty to represent the shortwave feedback and its nonlinearity. There are moreover discrepancies between modeled and observed α_{SW}^{-} and α_{SW}^{+} (Fig. 8) that may arise from (i) a biased spatial distribution of convective and subsident regions within Niño-3, (ii) errors in clouds radiative forcing representation in models or (iii) wrong (weak) nonlinearity in the atmospheric dynamical response to SST variations in terms of large-scale vertical motions (Lloyd et al 2012). Lloyd et al (2012) led an analysis for individual CMIP3 models in order to understand the origins of the discrepancies in modeled shortwave feedbacks. This can also be used for all CMIP5 models in order to provide a guideline for each model to work for a better representation of this important and complex damping term and its seasonal variations.

In order to better characterize the representation of ENSO in models and in particular to describe the full impact of the Bjerknes feedback on ENSO variability, a study of its interaction with the oceanic mean state and dynamics is needed. To diagnose the thermocline, the oceanic zonal advection and the Ekman pumping responses to anomalies of zonal wind stress is indeed decisive to work on the improvement of ENSO in climate models. The Jin et al (2006) BJ-index approach could be used to further analyze the simulation of ENSO processes in CMIP5. The BJ-index framework could be in addition a powerful tool to further investigate the importance of shortwave feedback nonlinearity on ENSO amplitude, still some work is needed in order to include such feedbacks nonlinearity in this simplified model.

Another implication of the relationship between shortwave feedback nonlinearity and ENSO amplitude (fig. 9) is that computing α_{SW} over a few years may help give an indication on the modeled ENSO amplitude, otherwise diagnosed from multi-century simulations. The shift of regime from mostly subsident to convective may moreover play a role in the phase locking of ENSO in the seasonal cycle (Fig. 10). The type of shortwave feedback is also shown to be related to the mean state (Fig. 11). The results of this study show that improving ENSO, the seasonal cycle and the mean state of a model all come together, suggesting that errors in the simulation of these phenomena share the same origin.

Finally, many of the new CGCMs are simulating much more processes than they did in CMIP3: aerosol indirect effect, stratosphere/troposphere interactions, land ice, flowing rivers, carbon cycle, ecosystems, and forcing by emissions rather than concentrations. This makes simulating Earth's climate more challenging by adding new potential feedbacks that can amplify biases, more uncertain model parameters to tune and more constraints when finalizing the model set up. In that sense, the fact that ENSO properties in CMIP5 are not degraded adds confidence in the modeling enterprise itself. This new generation of models hence holds promising new avenues for exploring the impacts of ENSO in Earth System Models.

Acknowledgements

We acknowledge the support from the European Union EUCLIPSE project (ENV/244067, FP7), the Agence Nationale pour la Recherche projects ANR-10-Blanc-616 METRO. We also acknowledge CMIP3 and CMIP5 modeling groups, ESG and PRODIGUER data distribution systems.

References

AchutaRao, K., and K. Sperber, 2006: ENSO simulations in coupled ocean-atmosphere models: Are the current models better? Climate Dyn., 27, 1-16.

Barnett, T. P., M. Latif, E. Kirk, and E. Roeckner, 1991: On ENSO physics. J. Climate, 4, 487–515.

Bjerknes, J., 1969: Atmospheric teleconnections from the equatorial Pacific. Mon. Wea. Rev., 97, 163–172.

Capotondi, A., A. Wittenberg, and S. Masina, 2006: Spatial and temporal structure of tropical Pacific interannual variability in 20th century coupled simulations. Ocean Modelling, 15, 274-298.

Chiang, J. C., S. E. Zebiak and M. A. Cane, 2001: Relative roles of elevated heating and surface temperature gradients in driving anomalous surface winds over tropical oceans, J. Atmos. Sciences, 58, 1371-1394.

Collins, M., et al., 2010: The impact of global warming on the tropical Pacific Ocean and El Niño. Nature Geosci., 3 (6), 391–397, URL http:// dx.doi.org/10.1038/ngeo868.

Gill, A. E., 1980: Some simple solutions for heat-induced tropical circulation, Quart. J. Roy. Meteor. Soc., 106, 447-462.

Gleckler P. J., K. E. Taylor, and C. Doutriaux, 2008: Performance metrics for climate models, J. Geophys. Research, 113, D06104, doi:10.1029/2007JD008972.

Guilyardi, E., and Coauthors, 2004: Representing El Niño in coupled ocean–atmosphere GCMs: The dominant role of the atmospheric component. J. Climate, 17, 4623–4629.

Guilyardi E., 2006: El Niño-mean state-seasonal cycle interactions in a multi-model ensemble, Climate Dyn., 26, 329-348.

Guilyardi, E., A. Wittenberg, A. Fedorov, M. Collins, C.Z. Wang, A. Capotondi, G.J. van Oldenborgh, and T. Stockdale (2009a): Understanding El Niño in ocean-atmosphere

General Circulation Models: Progress and challenges. Bull. Amer. Met. Soc., 90, 325–340.

Guilyardi E., P. Braconnot, F.-F. Jin, S. T. Kim, M. Kolasinski, T. Li and I. Musat (2009b). Atmosphere feedbacks during ENSO in a coupled GCM with a modified atmospheric convection scheme. J. Clim., 22, 5698-5718

Guilyardi E. and A. Wittenberg (2010). ENSO and tropical Pacific metrics for CMIP5. IPCC Expert meeting on Assessing and Combining Multi Model Climate Projections, Boulder, USA, January 2010

Guilyardi, E., W. Cai, M. Collins, A. Fedorov, F.-F. Jin, A. Kumar, D.-Z. Sun, A. Wittenberg (2012). CLIVAR workshop summary: New strategies for evaluating ENSO processes in climate models. Bull. Amer. Met. Soc., in press (due Feb 2012)

Harrison, D. E., and G. A. Vecchi, 1999: On the termination of El Niño, Geophys. Res. Lett., 26, 1593-1596.

Jiang, J. H. and coauthors 2012: Evaluation of cloud and water vapor simulations in CMIP5 climate models using NASA “A-Train” satellite observations, J. Geophys. Res., 117, D14105.

Jin, F.-F., 1997: An equatorial ocean recharge paradigm for ENSO. Part I: conceptual model, J. Atmos. Sci., 54, 811-829.

Jin, F.-F., S. T. Kim, and L. Bejarano, 2006: A coupled-stability index for ENSO. Geophys. Res. Lett., 33, L23708, doi:10.1029/ 2006GL027221.

Kim S. T., F. F. Jin, 2011: An ENSO stability analysis. Part II: results from the twentieth and twenty-first century simulations of the CMIP3 models, Clim Dyn, 36, 1609-1627.

Kim, D., J.-S. Kug, I.-S. Kang, F.-F. Jin, and A. T. Wittenberg, 2008: Tropical Pacific impacts of convective momentum transport in the SNU coupled GCM. Climate Dyn., 31, 213-226. doi:10.1007/s00382-007-0348-4.

Leloup, J., M. Lengaigne, and J.-P. Boulanger, 2008: Twentieth century ENSO characteristics in the IPCC database. Clim. Dyn., 30(2–3), 277–291, doi:10.1007/s00382-007-0284-3.

Lengaigne M., J.-P. Boulanger, C. Menkes and H. Spencer 2006: Influence of the seasonal cycle on the termination of El Niño events in a coupled general circulation model, J. Climate, 19, 1850-1868.

Lengaigne, M., and G. A. Vecchi, 2010: Contrasting the termination of moderate and extreme El Niño events in coupled general circulation models, Climate Dyn., 35, 299-313.

Lloyd, J., E. Guilyardi, H. Weller, and J. Slingo, 2009: The role of atmosphere feedbacks during ENSO in the CMIP3 models. Atmos. Sci. Lett., 10, 170–176.

Lloyd, J., E. Guilyardi and H. Weller 2011: The role of atmosphere feedbacks during ENSO in the CMIP3 models, Part II: using AMIP runs to understand the heat flux feedback mechanisms, Clim. Dyn. 37, 1271- 1292, DOI: 10.1007/s00382-010-0895

Lloyd, J., E. Guilyardi and H. Weller 2011: The role of atmosphere feedbacks during ENSO in the CMIP3 models, Part III: The shortwave feedback, J. Climate, 25, 4275-4293.

Marti O., P. Braconnot, J.-L. Dufresne, J. Bellier, R. Benshila, S. Bony, P. Brockmann, P. Cadule, A. Caubele, F. Codron, et al 2010: Key features of the IPSL ocean atmosphere model and its sensitivity to atmospheric resolution, Clim. Dyn., 34, 1-26.

McPhaden, M. J.; Zebiak, S. E. & Glantz, M. H. (2006). ENSO as an Integrating Concept in Earth Science science, 314, 1739-1745

Meehl, G. A., C. Covey, T. Delworth, M. Latif, B. McAvaney, J. F. B. Mitchell, R. J. Stouffer, and K. E. Taylor, 2007: The WCRP CMIP3 multimodel dataset, Bull. American Meteor. Soc., September 2007, 1383-1394.

Naylor R.L., D.S. Battisti, D.J. Vimont, W.P. Falcon and M.B. Burke 2007 : assessing risks of climate variability and climate change for indonesian rice agriculture, PNAS, 104, 7752-7757.

Neale, R. B., Richter, J. H., & Jochum, M. (2008). The Impact of Convection on ENSO: From a Delayed Oscillator to a Series of Events. Journal of Climate, 21(22), 5904–5924. doi:10.1175/2008JCLI2244.1

Nichol J., 1997: Bioclimatic impacts of the 1994 smoke haze event in southeast asia, Atmos, Envir., 31, 8, 1209-1219

Philander, S., D. Gu, G. Lambert, T. Li, D. Halpern, N.-C. Lau, and R. Pacanowski, 1996: Why the ITCZ is mostly north of the equator. J. Climate, 9, 2958–2972.

Picaut J., F. Masia, and Y. du Penhoat, 1997:An advective-reflective conceptual model for the oscillatory nature of ENSO, Science, 277, 663-666.

Rasmusson, E., and T. Carpenter, 1982: Variations in tropical sea surface temperature and surface wind fields associated with the Southern Oscillation/El Niño, Mon. Wea. Rev., 110, 354-384.

Rayner NA, Parker DE, Horton EB, Folland CK, Alexander LV, Rowell DP, Kent EC, Kaplan A (2003) Global analyses of sea surface temperature, sea ice, and night marine air temperature since the late nineteenth century. J Geophys Res (Atmos) 108:4407

Stevenson, S., Fox-Kemper, B., Jochum, M., Rajagopalan, B., & Yeager, S. G. (2010). ENSO Model Validation Using Wavelet Probability Analysis. Journal of Climate, 23(20), 5540–5547. doi:10.1175/2010JCLI3609.1

Suarez, M. J., and P. S. Schopf, 1988: A delayed action oscillator for ENSO, J. Atmos. Sci., 45, 3283-3287.

Sun, D.-Z., Y. Yu, and T. Zhang, 2009: Tropical water vapor and cloud feedbacks in climate models: a further assessment using coupled simulations, J. Climate, 22, 1287-1304.

Taylor K. E., R. J. Stouffer, and G. A. Meehl, 2012: Overview of CMIP5 and the experiment design, Bull. American Meteor. Soc., april 2012, 485-498.

Toniazzo, T., M. Collins, and J. Brown, 2008: The variation of ENSO characteristics associated with atmospheric parameter perturbations in a coupled model. Climate Dyn., 30, 643– 656.

Tziperman, E., M. A. Cane, S. E. Zebiak, Y. Xue, and B. Blumenthal, 1998: Locking of El Niño's peak time to the end of the calendar year in the delayed oscillator picture of ENSO, J. Climate, 11, 2191-2199.

Uppala et al. (2005) The ERA-40 Re-analysis. Quart J R Met Soc 131:2961–3012

Van Oldenborgh G. J., S. Y. Philip, and M. Collins, 2005: El Niño in a changing climate: a multi-model study, Ocean Sc. 1, 81-95.

Vecchi, G. A., and A. T. Wittenberg, 2010: El Niño and our future climate: Where do we stand? Wiley Interdisciplinary Reviews: Climate Change, 1, 260-270. doi:10.1002/wcc.33

Wang B. and S. I. An, 2002: A mechanism for decadal changes of ENSO behavior: roles of background wind changes, Climate Dyn., 18, 475-486.

Wang C. And J. Picaut 2004: Understanding ENSO physics – A review, Geophys. Monogr. AGU 147, 21-48.

Watanabe, M., Suzuki, T., O'ishi, R., Komuro, Y., Watanabe, S., Emori, S., Takemura, T., et al. (2010). Improved Climate Simulation by MIROC5: Mean States, Variability, and Climate Sensitivity. Journal of Climate, 23(23), 6312–6335. doi:10.1175/2010JCLI3679.1

Watanabe, M., M. Chikira, Y. Imada, and M. Kimoto 2011: Convective control of ENSO simulated in MIROC, J. Climate, 24, 543-562.

Webster, P. J., V. Magaña, T. N. Palmer, J. Shukla, R. A. Tomas, M. Yanai, and T. Yasunari, 1998: Monsoons: Processes, predictability and the prospects for prediction. J. Geophys. Res., 103, 14451-14510.

Weisberg, R. H., and C. Wang, 1997: A western Pacific oscillator paradigm for the El Niño-Southern Oscillation, Geophys. Res. Lett., 27, no7, 779-782.

Wittenberg, A. T., T. Rosati, and I. Held, 2003: ENSO in the GFDL coupled model. Eighth Annual CCSM Workshop, Breckenridge, CO, UCAR. [Available online at http://www.gfdl.noaa.gov/atw/research/conf/ccsm8/talk.pdf.]

Wittenberg, A. T. (2009), Are historical records sufficient to constrain ENSO simulations?, Geophys. Res. Lett., 36, L12702, doi:10.1029/2009GL038710.

Wu, X., L. Deng, X. Song, G. Vettoretti, W. R. Peltier, and G. J. Zhang, 2007: Impact of a modified convective scheme on the Madden-Julian oscillation and El Niño–Southern Oscillation in a coupled climate model. Geophys. Res. Lett., 34, L16823, doi:10.1029/2007GL030637.

Xie, P., and P.A. Arkin, 1997: Global precipitation: A 17-year monthly analysis based on gauge observations, satellite estimates, and numerical model outputs. Bull. Amer. Meteor. Soc., 78, 2539 - 2558.

Xie, S.-P., 2005: The shape of continents, air-sea interaction, and the rising branch of the Hadley circulation. The Hadley Circulation: Present, Past and Future, H. F. Diaz and R. S. Bradley, Eds., Advances in Global Change Research, Vol. 21, Kluwer Academic Publishers, 121–152

Yu J.-Y. and S. T. Kim, 2010: Identification of Central-Pacific and Eastern-Pacific types of ENSO in CMIP3 models, Geophys. Res. Lett., 37, L15705.

Yu, L., and R. A. Weller, 2007: Objectively Analyzed air-sea heat Fluxes for the global ice-free oceans (1981–2005). Bull. Ameri. Meteor. Soc., 88, 527–539

Zebiak, S. E., and M. A. Cane, 1987: A model El Niño–Southern Oscillation. Mon. Wea. Rev., 115, 2262–2278.

Tables

Table1. CMIP3 and CMIP5 official model names per modeling centers. The number of years of pre-industrial control run available for this study and the corresponding type of α_{SW} (see §5) are also reported. The "-" stands for model (or necessary data) not available.

		CMIP3			CMIP5		
Modeling center number	Modeling center	Model	Run length (years)	α_{SW} type	Model	Run length (years)	α_{SW} type
1	BCC	-	-	-	BCC-CSM1	500	SUB
2	BCCR	BCCR-BCM2.0	250	MIX	-	-	-
3	BNU	-	-	-	BNU-ESM	559	MIX
4	CCCma	CGCM3.1 (a) CGCM3.1-t63 (b)	1000 350	CONV CONV	CanESM2	996	MIX
5	CMCC	-	-	-	CMCC-CM	330	CONV
6	CNRM-CERFACS	CNRM-CM3	500	MIX	CNRM-CM5	850	CONV
7	CSIRO-QCCCE	CSIRO-Mk3.0 (a) CSIRO-Mk3.5 (b)	380 910	MIX MIX	CSIRO-Mk3.6	500	SUB
8	FIO	-	-	-	FIO-ESM	800	MIX
9	GFDL	GFDL2.0 (a) GFDL2.1 (b)	500 500	MIX MIX	GFDL-CM3 (a) GFDL-ESM2G (b) GFDL-ESM2M (c)	500 500 500	MIX SUB MIX
10	GISS	GISS-AOM (a) GISS-EH (b) GISS-ER (c)	251 400 500	CONV SUB CONV	GISS-E2-H (a) GISS-E2-R (b)	480 300	CONV CONV
11	IAP (LASG & CESS)	FGOALSg1.0	350	MIX	FGOALSg2 (a) FGOALSs2 (b)	900 501	CONV SUB
12	INGV	INGV-ECHAM4	100	-	-	-	-
13	INM	INM-CM3.0	330	SUB	INM-CM4	500	SUB
14	IPSL	IPSL-CM4	500	MIX	IPSL-CM5A-LR (a) IPSL-CM5A-MR (b) IPSL-CM5B-LR (c)	1000 300 300	SUB SUB MIX
15	MIROC	MIROC3.2 MR (a) MIROC3.2 HR (b)	500 100	SUB CONV	MIROC4h (a) MIROC5 (b) MIROC-ESM (c) MIROC-ESM-CHEM (d)	100 670 531 255	CONV CONV SUB SUB
16	MIUB	ECHO-G	341	MIX	-	-	-
17	MOHC	HadCM3 (a) HadGEM1 (b)	342 240	SUB SUB	HadGEM2-ES (a) HadGEM2-CC (b)	240 575	SUB SUB
18	MPI	ECHAM5/MPI-OM	506	MIX	MPI-ESM-LR (a) MPI-ESM-MR (b) MPI-ESM-P (c)	1000 1000 1156	SUB SUB SUB
19	MRI	MRI-CGCM2.3.2	350	SUB	MRI-CGCM3	500	SUB
20	NCAR	CCSM3.0 (a) NCAR-PCM1 (b)	230 500	SUB SUB	CCSM4	501	MIX
21	NCC	-	-	-	NorESM1-M (a) NoeESM1-ME (b)	501 252	MIX MIX
22	NSF-DOE-NCAR	-	-	-	CESM1-FASTCHEM (a) CESM1-WACCM (b)	222 200	MIX MIX

Table 2. Average precipitation response to ENSO in Niño-4, Bjerknes feedbacks, ENSO seasonality metric (Fig. 3b) and the March-April-May shortwave feedback for SUB, MIX and CONV-type models. The standard deviation is given in parenthesis.

	SUB-type	MIX-type	CONV-type
Precip std. Dev. in Niño-4 (mmh^{-1}/C)	1.2 (0.5)	2.2 (0.65)	1.63 (0.6)
Bjerknes Feedback (10^{-3} Nm^{-2}/C)	6.2 (1.8)	7.3 (1.6)	9.1 (2.2)
ENSO seasonality metric : Niño-3 SST std. Dev. (NDJ/MAM)	1.08 (0.23)	1.21 (0.35)	1.28 (0.24)
Average March-April-May shortwave feedback (α_{SW}, in Wm^{-2}/C)	3.99 (3.91)	-3.83 (4.13)	-9.56 (5.97)

Figure Captions:

Figure 1. ENSO metrics for pre-industrial control simulations - CMIP3 (blue) and CMIP5 (red). (a) and (b) SSTA std. dev. in Niño-3 and Niño-4 (°C), (c) precipitation std dev. in Niño-4 (mm/day), (d) RMS error of Niño-3 SSTA power spectrum , (°C^2). Reference datasets, shown as black solid circles and dashed lines, are HadISST1.1 for (a), (b), (d) and CMAP for (c) The CMIP3 and CMIP5 multi-model mean are shown as squares on the left of each panel with the whiskers representing the inter-model standard deviation.

Figure 2. ENSO spectral characteristics diagnosed from Niño-3 SST anomalies: (a) Examples of spectra with HadISST1.1 (green), two CMIP3 (blue) and CMIP5 (red) models peaking respectively in the 1-3 year band and the 3-8 band (vertical dashed black lines locate 1, 3 and 8 years) and (b) spectral shape metric defined as the ratio between the power in the 3-8 years band and in the 1-3 years band for HadISST1.1 (black), CMIP5 models (light red) and CMIP3 models (light blue), the squares represent the corresponding average with whiskers representing the inter-model standard deviation.

Figure 3. ENSO seasonality diagnosed from Niño-3 SST anomalies: (a) Monthly average standard deviation of the SST anomalies (°C) and (b) Seasonality metrics defined as the ratio between the November-January (NDJ) and the March-May (MAM) average standard deviation of the SST anomalies for HadISST1.1 (black), CMIP5 models (light red) and CMIP3 models (light blue), the squares represent the corresponding average with whiskers representing the inter-model standard deviation.

Figure 4. Percentage of occurrence of maximum SST anomaly in the western (150°E-170°W, 5°S-5°N), central (170°W-130°W, 5°S-5°N) and eastern (130°W-90°W, 5°S-5°N) Pacific

Ocean for El Niño (a-d) and La Niña (e-g) events during there onset phase (a and d), peak phase (b and e) and termination phase (c and f) for the observations (black) and CMIP3 (blue) and CMIP5 ensembles averages (red) and standard deviation among the models (whiskers), (g) As (b) but for all individual models.

Figure 5. ENSO mean tropical Pacific metrics for pre-industrial control simulations - CMIP3 (blue) and CMIP5 (red). (a) SST RMS error in tropical Pacific (in °C), (b) SST annual cycle amplitude in Niño-3 (in °C), (c) zonal wind stress spatial RMS error over equatorial Pacific (5°N-5°S; in $10^{-3}Nm^{-2}$), (d) precipitation spatial RMS error over tropical Indo-Pacific (30°N-30°S, in mm/day), (e) net surface heat flux RMS error in Niño-3 ($W.m^{-2}$). Reference datasets, shown as black solid circles and dashed lines, are HadISST1.1 for (a) and (b); ERA40 for (c); CMAP for (d); and OAFlux for (e). See models and centers legend in Fig. 1 and Table 1. The CMIP3 and CMIP5 multi-model mean are shown as squares on the left of each panel with the whiskers representing the model standard deviation.

Figure 6. Average (a) SST (K) and (b) zonal surface wind stress (Nm^{-2}) at the equator (5°S-5°N) in the Pacific Ocean for ERA-40 (black) and CMIP3 (blue) and CMIP5 (red) ensemble mean. The inter model standard deviation is shaded in light color.

Figure 7. Atmosphere feedbacks during ENSO for pre-industrial control simulations - CMIP3 (blue) and CMIP5 (red). (a) Bjerknes feedback, computed as the regression of Niño 4 wind stress over Niño3 SST (10^{-3} $N.m^{-2}.°C^{-1}$); (b) heat flux feedback, computed as the regression of total heat flux over SST in Niño3 ($W.m^{-2}.°C^{-1}$); (c) Shortwave component of (b); (d) Latent heat flux component of (b). Reference datasets, shown as black solid circles and dashed lines, are ERA40 for (a) and OAFlux for (b), (c) and (d). See models and centers legend in Fig. 1

and Table 1. The CMIP3 and CMIP5 multi-model mean are shown as squares on the left of each panel with the whiskers representing the model standard deviation.

Figure 8. Shortwave monthly anomalies in Niño3 as a function of SST monthly anomalies in Niño3 for (a) IPSL-CM5A-MR (dots) and segmented linear fits (blue), (b) Reference data (green dots, HadISST and OAFlux for 1984-1999) and FIOESM (gray dots) and corresponding segmented linear fits (green and black lines), and (c) MIROC5 (dots) and segmented linear fits (red). (d), (e) and (f) show the segmented linear fits for the CMIP3 and CMIP5 models according to their types: (d) SUB-type: α_{SW} always positive, (e) MIX-type: α_{SW} changing sign and (f) CONV-type: α_{SW} always negative.

Figure 9. Scatterplot of Niño-3 SST anomalies standard deviation as a function of nonlinearity in alpha shortwave feedback. The colors represents the type of alpha SW. alpha SW nonlinearity is quantified by taking a_{SW}^{-} - a_{SW}^{+}. The green square is the reference (HadISST and OAFlux on 1984-1999).

Figure 10. Average monthly (a) shortwave feedback ($Wm^{-2}.°C^{-1}$), and (b) scatterplot of the seasonality metric against March-April-May average shortwave feedback for corresponding reference datasets (green), SUB-type models (blue), MIX-type models (black) and CONV-type models (red). The inter model standard deviation is plotted in light color.

Figure 11. Average (a) SST (°C) and (b) zonal surface wind stress ($N.m^{-2}$) at the equator (5°S-5°N) in the Pacific Ocean for ERA-40 (green) and SUB-type models (blue), MIX-type models (black) and CONV-type models (red) ensemble mean. The inter model standard deviation for each model type is plotted in light color.

Figure 12. Scatterplots of nonlinearity in shortwave feedback as a function of the difference between each model and Reynolds (REF) of (a) the average SST in the equatorial Pacific Ocean (180°E-240°E, 5°S-5°N) and (b) the average zonal SST gradient between (160°E-200°E, 5°S-5°N) and (220°E-240°E, 5°S-5°N). The colors refer the type of the models (blue) SUB-type, (black) MIX-type and (red) CONV-type.

Figure 13. ENSO simulation performances for each model of CMIP3 (upper) and CMIP5 (lower) designated by the name of the modeling group and a letter (see table 1 and figure 1). Four primary scores are used to depict the ENSO quality: the normalized error (cf. (1), no unit, a zero value indicating a perfect agreement with observations for that measure) of the SSTA std. dev. in Niño-3 (Amplitude), of the percentage of El Niño peak in eastern Pacific (Structure), of the ratio between power in 3-8 years over 1-3 years (Spectrum) and of the ratio of average SSTA standard deviation in Niño-3 in NDJ over MAM (Seasonality). The ENSO score is then defined as the average of these primary scores. Thus, the lower the ENSO score, the better the model represents the basic characteristics of ENSO. Four primary scores depict the atmosphere feedbacks and consist in the normalized error of μ, α and its shortwave and latent heat components. The overall Feedback score (FB SCORE) is the average of these scores. The grey squares spot the metrics that could not be calculated because of the lack of data. The corresponding score is not computed for these models.

Figure 14. Scatterplots of ENSO score versus Feedback score (see Fig. 13) for each CMIP5 (large labels) and CMIP3 (small labels) model. The color refers to the type of the model: CONV (red), MIX (black) and SUB (blue). “c3” is added to the model name for CMIP3 models.

Figure 1

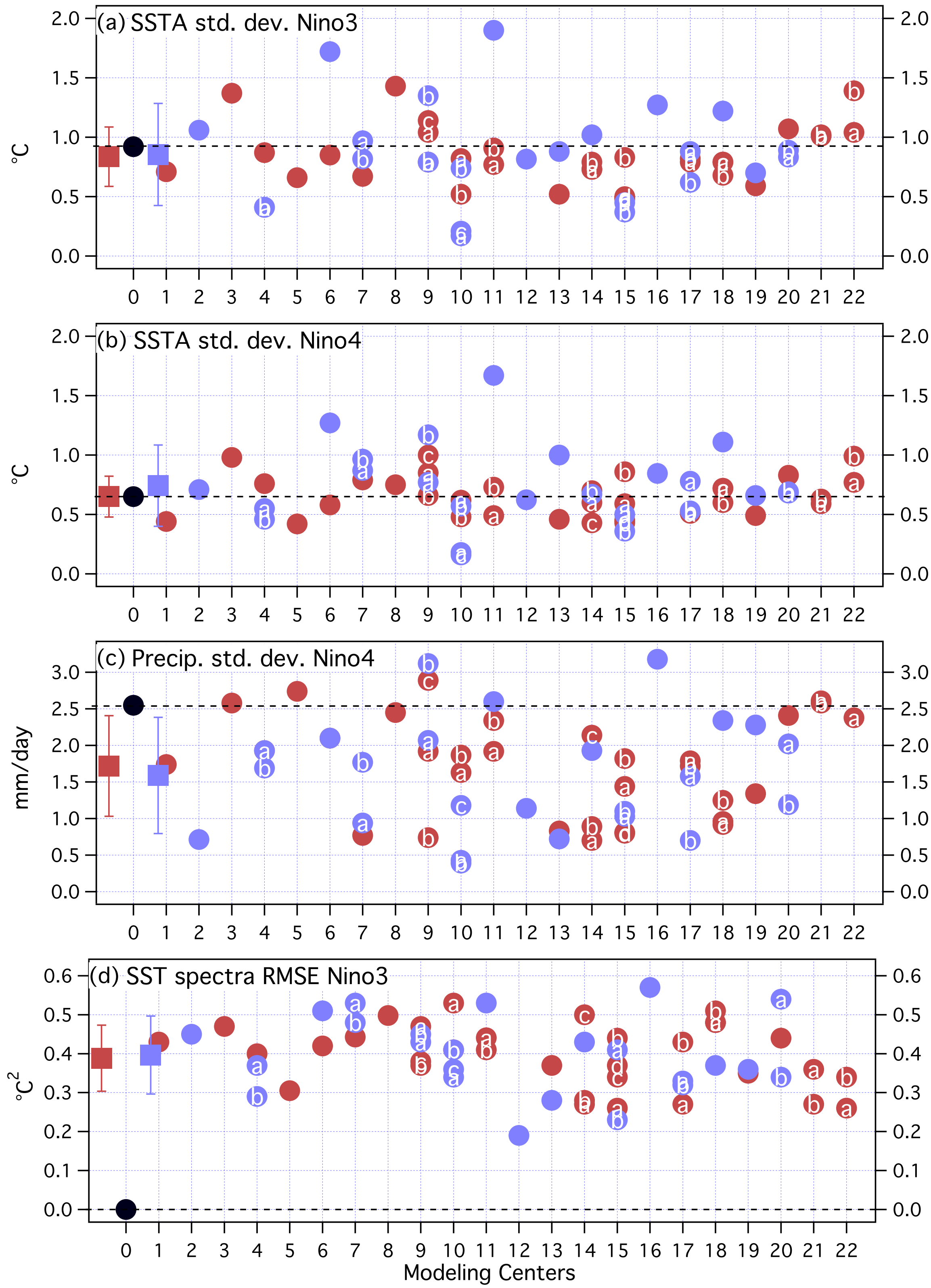

0-CMIP3
0-CMIP5
0-Ref.

1- BCC
- BCC-CSM1
2- BCCR
- BCCR-BCM2.0
3- BNU
- BNU-ESM
4- CCCma
a- CGCM3.1
b- CGCM3.1-t63
- CanESM2
5- CMCC
- CMCC-CM
6- CNRM
- CNRM-CM3
- CNRM-CM5
7- CSIRO
a- CSIRO-Mk-3.0
b- CSIRO-Mk-3.5
- CSIRO-Mk3.6
8- FIO
- FIO-ESM
9- GFDL
a- GFDL2.0
b- GFDL2.1
a- GFDL-CM3
b- GFDL-ESM2G
c- GFDL-ESM2M
10- GISS
a-GISS-AOM
b-GISS-EH
c-GISS-ER
a-GISS-E2-H
b-GISS-E2-R
11- IAP
- FGOALSg1
a- FGOALS-g2 (IAP+CESS)
b- FGOALS-s2
12- INGV
- INGV-ECHAM4
13- INM
- INM-CM3
- INM-CM4
14- IPSL
- IPSL-CM4
a- IPSL-CM5A-LR
b- IPSL-CM5A-MR
c- IPSL-CM5B-LR
15-MIROC
a- MIROC3.2-MR
b- MIROC3.2-HR
a- MIROC4h
b- MIROC5
c- MIROC-ESM
d- MIROC-ESM-CHEM
16- MIUB
- ECHO-G
17- MOHC
a- HadCM3
b- HadGEM1
a- HadGEM2-ES
b- HadGEM2-CC
18- MPI
- ECHAM5/MPI-OM
a- MPI-ESM-LR
b- MPI-ESM-MR
c- MPI-ESM-P
19- MRI
- MRI-CGCM2.3.2
- MRI-CGCM3
20- NCAR
- CCSM4
a- CCSM3
b- PCM1
21- NCC
a-NorESM-M
b-NorESM-ME
22-NSF-DOE-NCAR
a- CESM1-FAST-CHEM
b- CESM1-WACCM

Figure 2

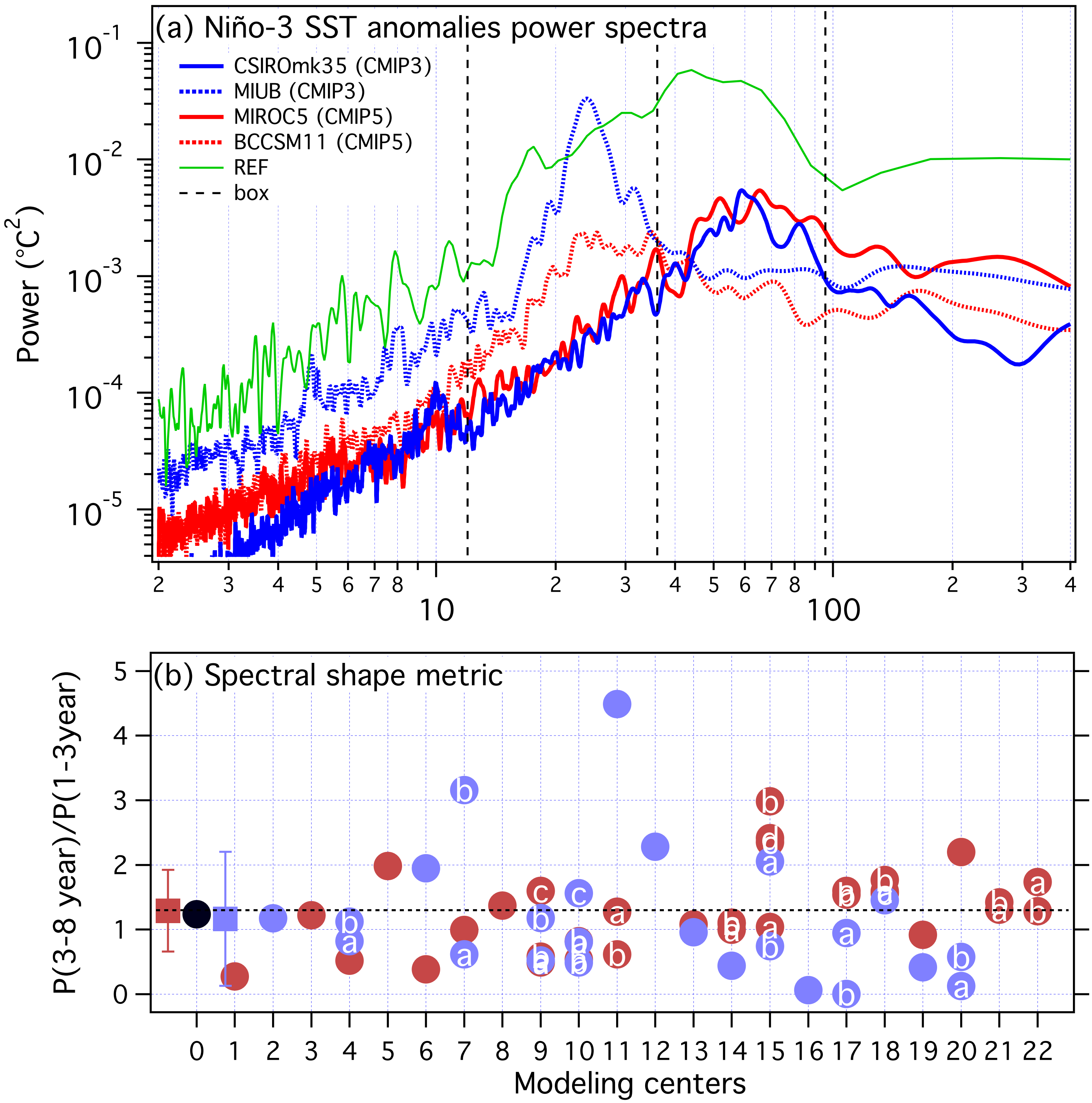
(a) Niño-3 SST anomalies power spectra
CSIROmk35 (CMIP3)
MIUB (CMIP3)
MIROC5 (CMIP5)
BCCSM11 (CMIP5)
REF
box
Power (°C^2)
10^{-1}
10^{-2}
10^{-3}
10^{-4}
10^{-5}
2 3 4 5 6 7 8 10 2 3 4 5 6 7 8 100 2 3 4
(b) Spectral shape metric
P(3-8 year)/P(1-3year)
0 1 2 3 4 5
0 1 2 3 4 5 6 7 8 9 10 11 12 13 14 15 16 17 18 19 20 21 22
Modeling centers

Figure 3

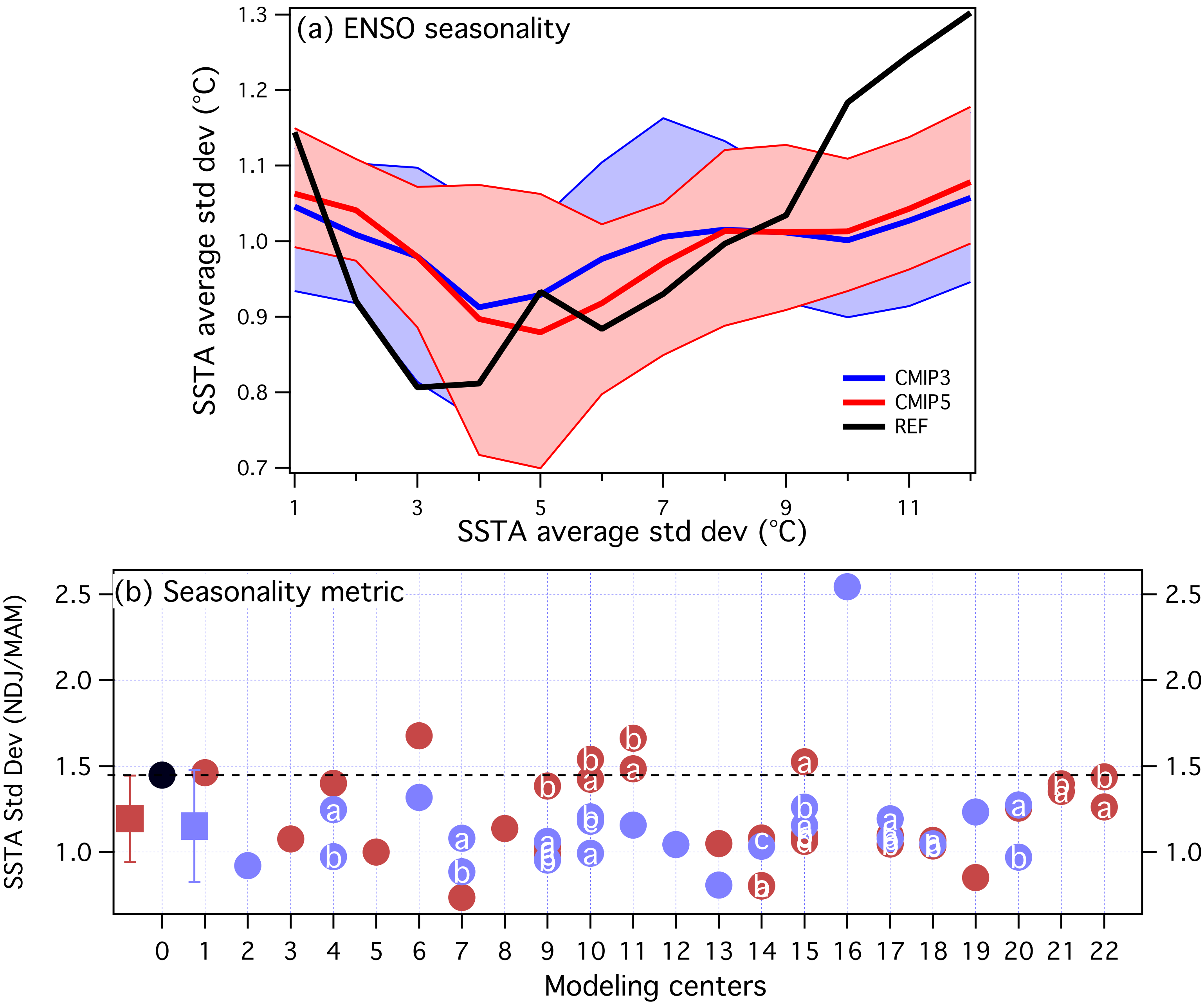

(a) ENSO seasonality
SSTA average std dev (°C)
1.3
1.2
1.1
1.0
0.9
0.8
0.7
1
3
5
7
9
11
SSTA average std dev (°C)
CMIP3
CMIP5
REF
(b) Seasonality metric
SSTA Std Dev (NDJ/MAM)
2.5
2.0
1.5
1.0
0 1 2 3 4 5 6 7 8 9 10 11 12 13 14 15 16 17 18 19 20 21 22
Modeling centers

Figure 4

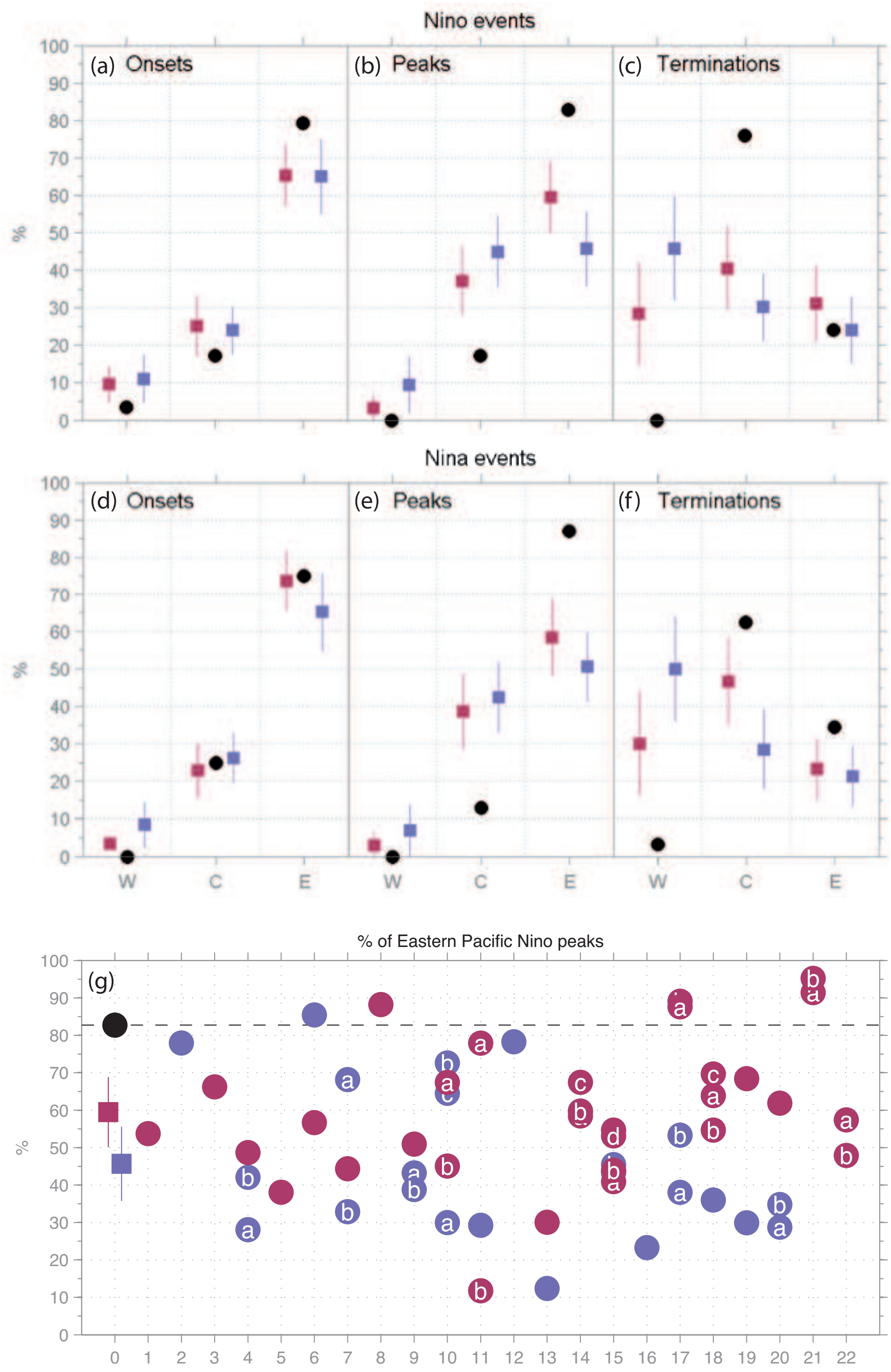

Nino events
(a) Onsets
(b) Peaks
(c) Terminations
Nina events
(d) Onsets
(e) Peaks
(f) Terminations
%
W
C
E
% of Eastern Pacific Nino peaks
(g)

Figure 5

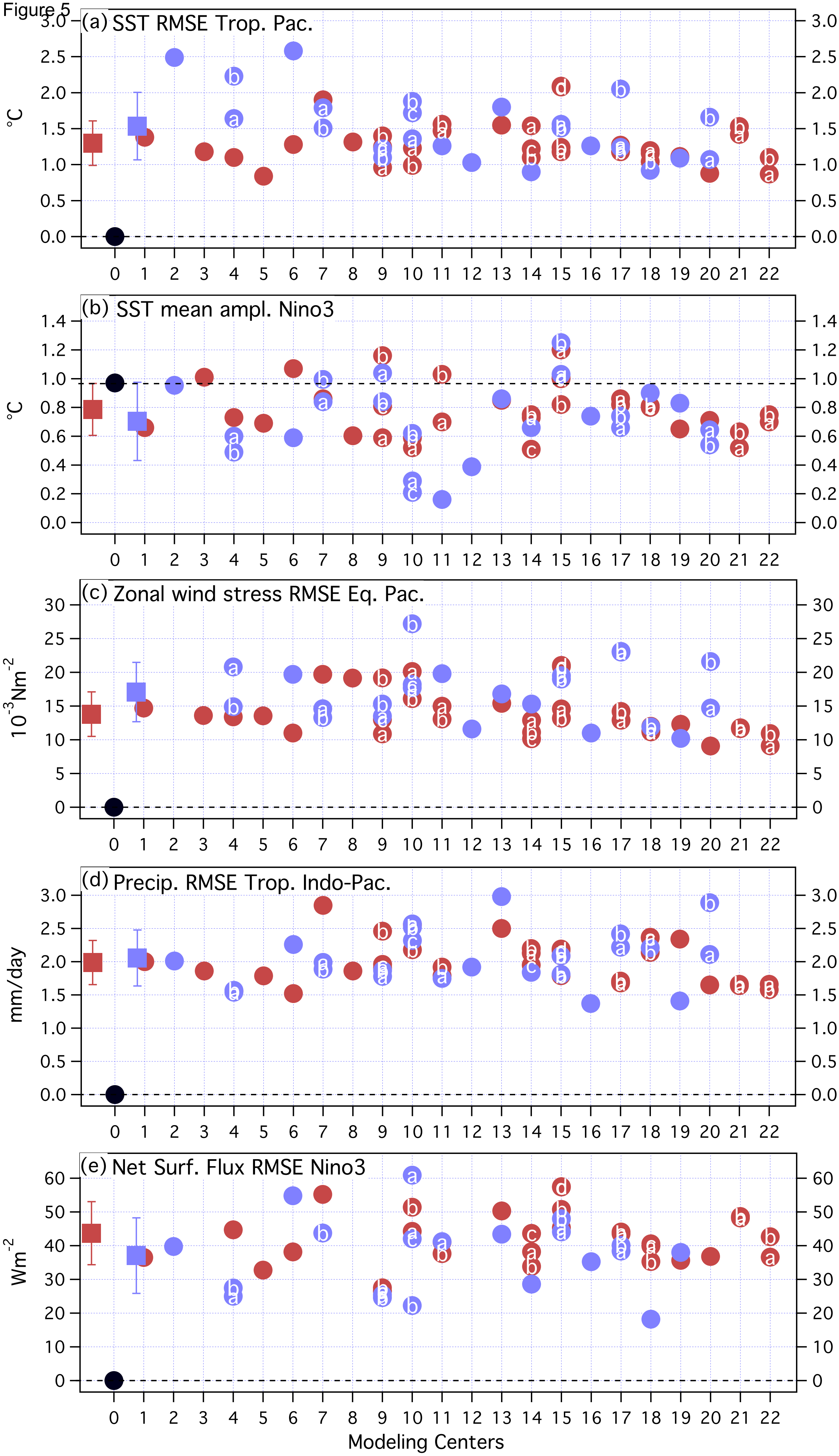
(a) SST RMSE Trop. Pac.
°C
(b) SST mean ampl. Nino3
°C
(c) Zonal wind stress RMSE Eq. Pac.
10^-3 Nm^-2
(d) Precip. RMSE Trop. Indo-Pac.
mm/day
(e) Net Surf. Flux RMSE Nino3
Wm^-2
Modeling Centers

Figure 6

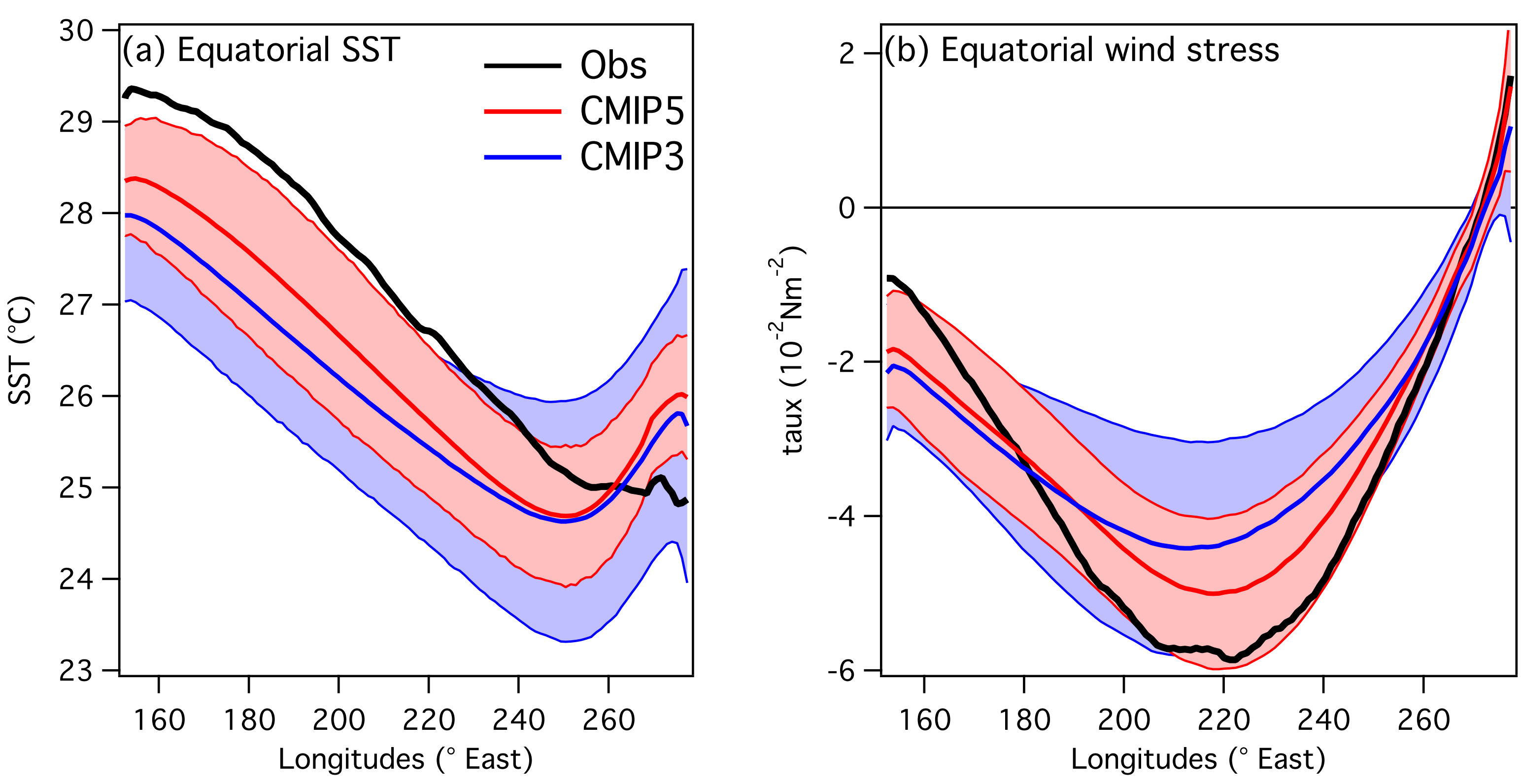

(a) Equatorial SST
Obs
CMIP5
CMIP3
SST (°C)
30
29
28
27
26
25
24
23
160
180
200
220
240
260
Longitudes (° East)
(b) Equatorial wind stress
taux ($10^{-2}Nm^{-2}$)
2
0
-2
-4
-6
160
180
200
220
240
260
Longitudes (° East)

Figure 7

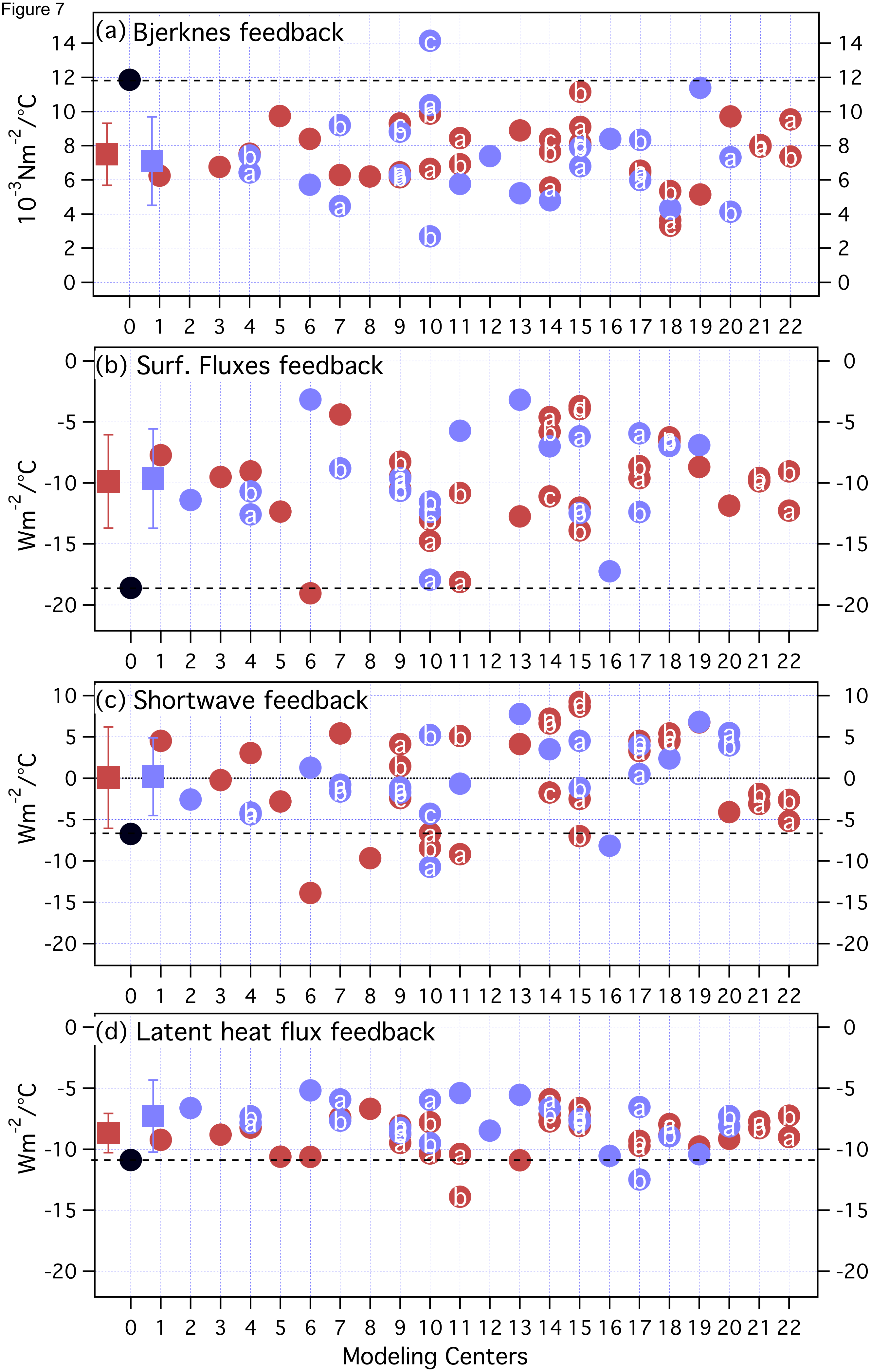
(a) Bjerknes feedback
$10^{-3}Nm^{-2}/°C$
(b) Surf. Fluxes feedback
$Wm^{-2}/°C$
(c) Shortwave feedback
$Wm^{-2}/°C$
(d) Latent heat flux feedback
$Wm^{-2}/°C$
Modeling Centers

Figure 8

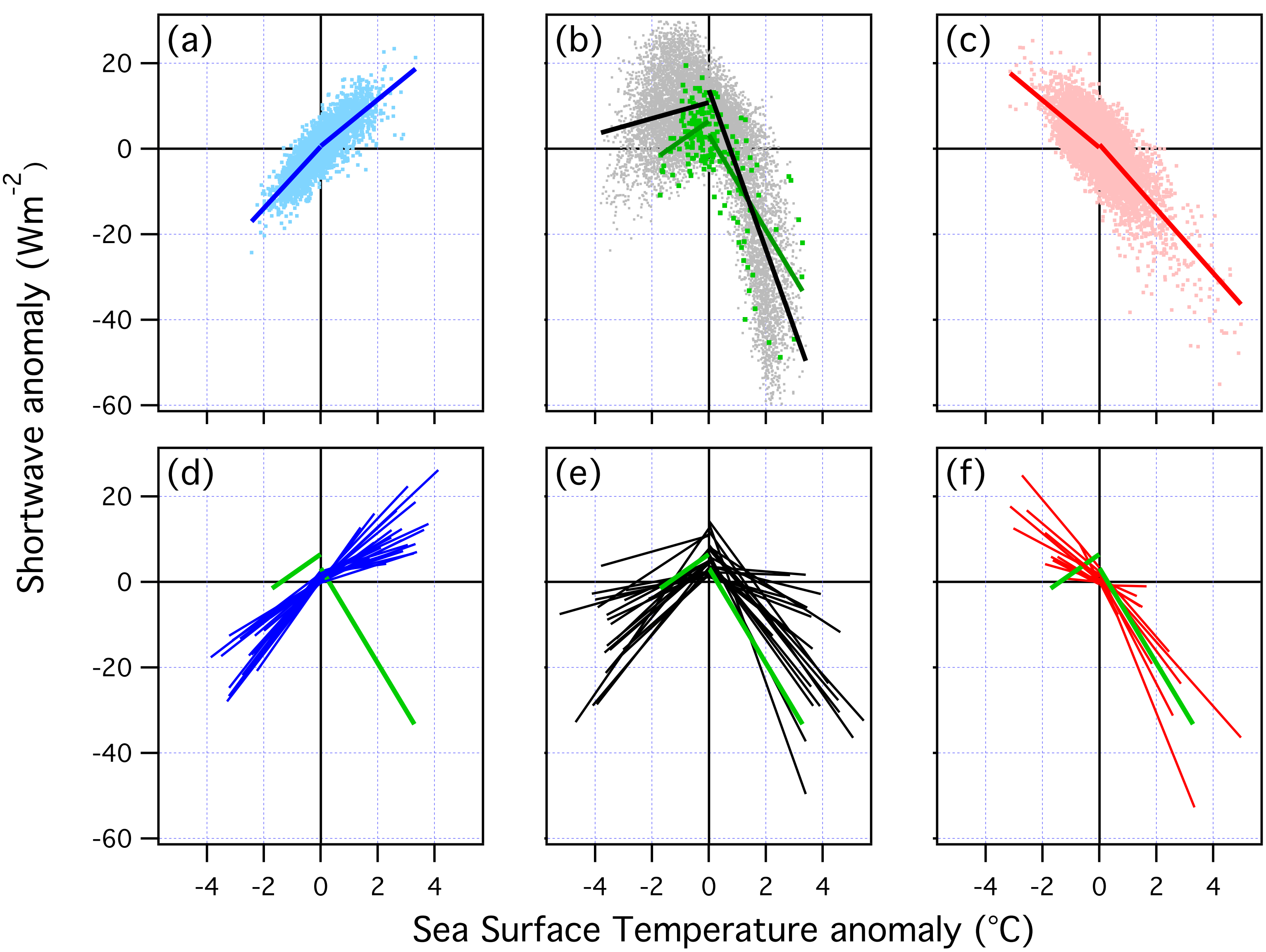
(a)
(b)
(c)
(d)
(e)
(f)
20
0
-20
-40
-60
-4
-2
0
2
4
Shortwave anomaly (Wm^{-2})
Sea Surface Temperature anomaly (°C)

Figure 9

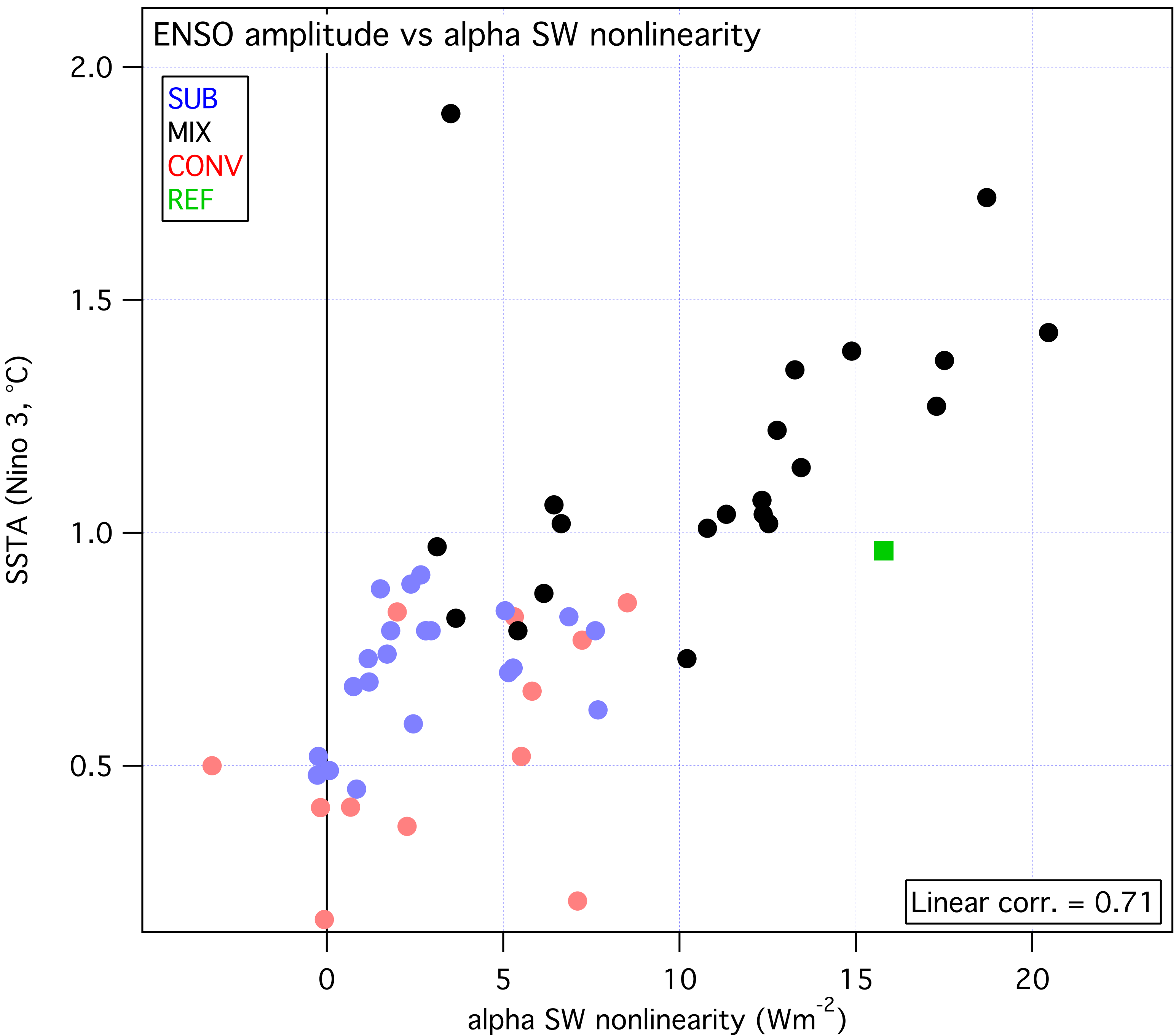
ENSO amplitude vs alpha SW nonlinearity
SUB
MIX
CONV
REF
Linear corr. = 0.71
SSTA (Nino 3, °C)
2.0
1.5
1.0
0.5
0
5
10
15
20
alpha SW nonlinearity (Wm^-2)

Figure 10

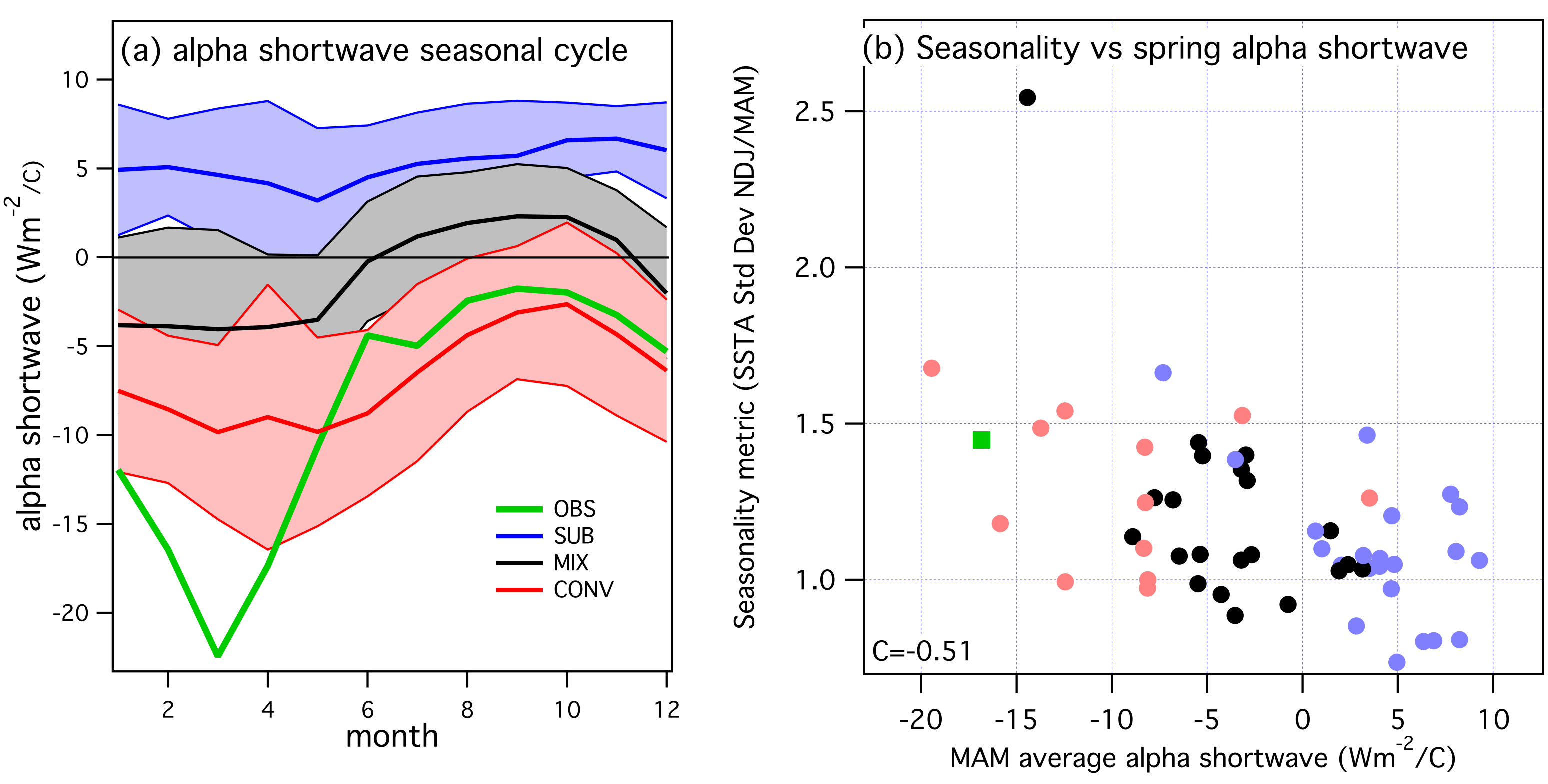

(a) alpha shortwave seasonal cycle
alpha shortwave (Wm^{-2}/C)
month
OBS
SUB
MIX
CONV
(b) Seasonality vs spring alpha shortwave
Seasonality metric (SSTA Std Dev NDJ/MAM)
MAM average alpha shortwave (Wm^{-2}/C)
C=-0.51

Figure 11

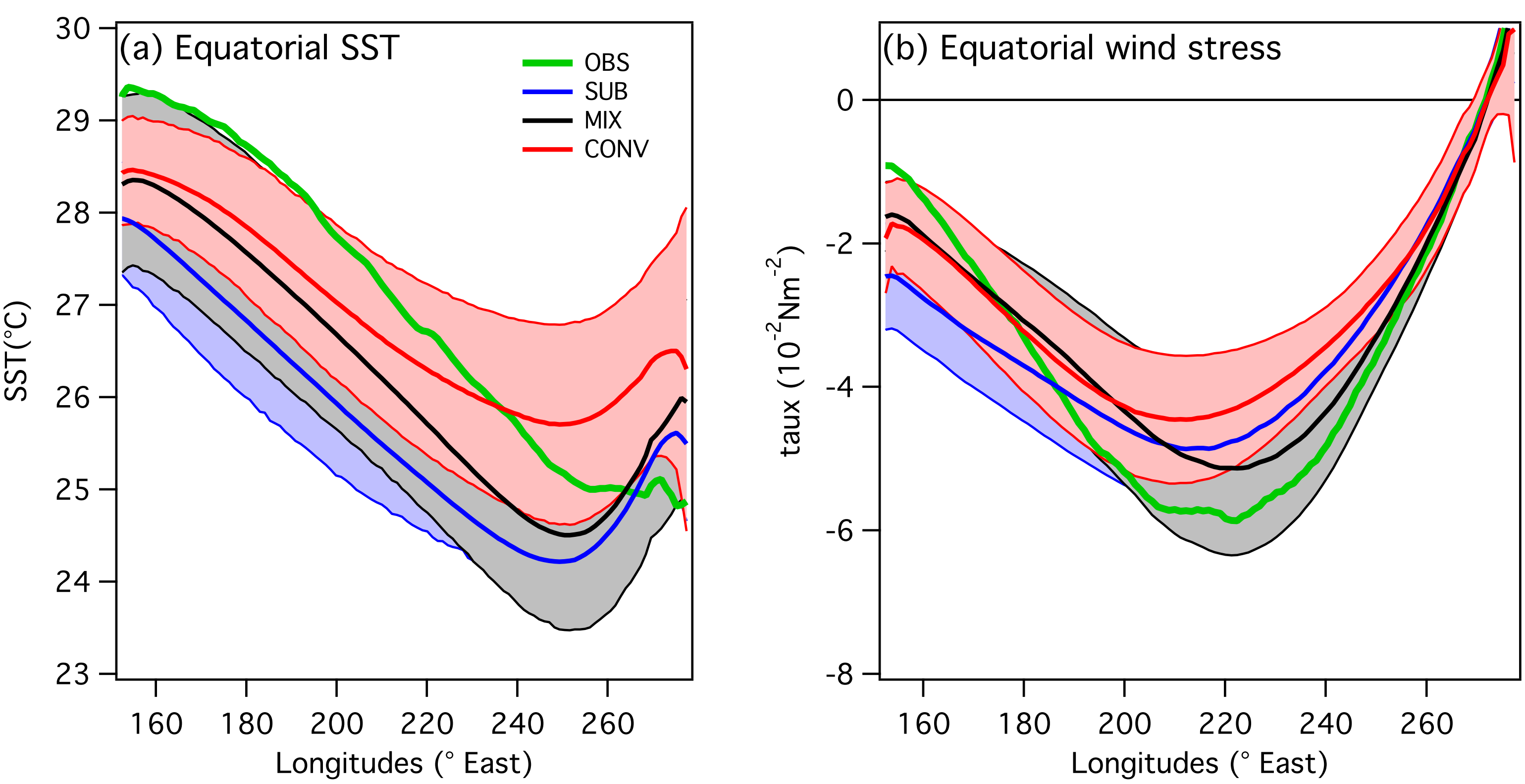
(a) Equatorial SST
OBS
SUB
MIX
CONV
SST(°C)
30
29
28
27
26
25
24
23
160
180
200
220
240
260
Longitudes (° East)
(b) Equatorial wind stress
taux ($10^{-2}Nm^{-2}$)
0
-2
-4
-6
-8
160
180
200
220
240
260
Longitudes (° East)

Figure 12

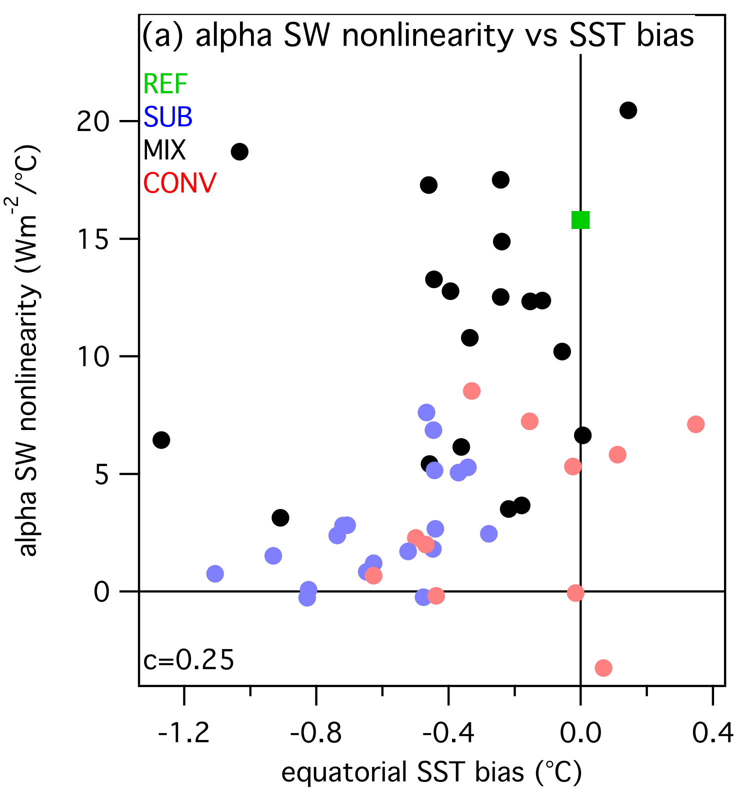

(a) alpha SW nonlinearity vs SST bias
REF
SUB
MIX
CONV
c=0.25
alpha SW nonlinearity (Wm^-2 /°C)
equatorial SST bias (°C)
-1.2
-0.8
-0.4
0.0
0.4
20
15
10
5
0

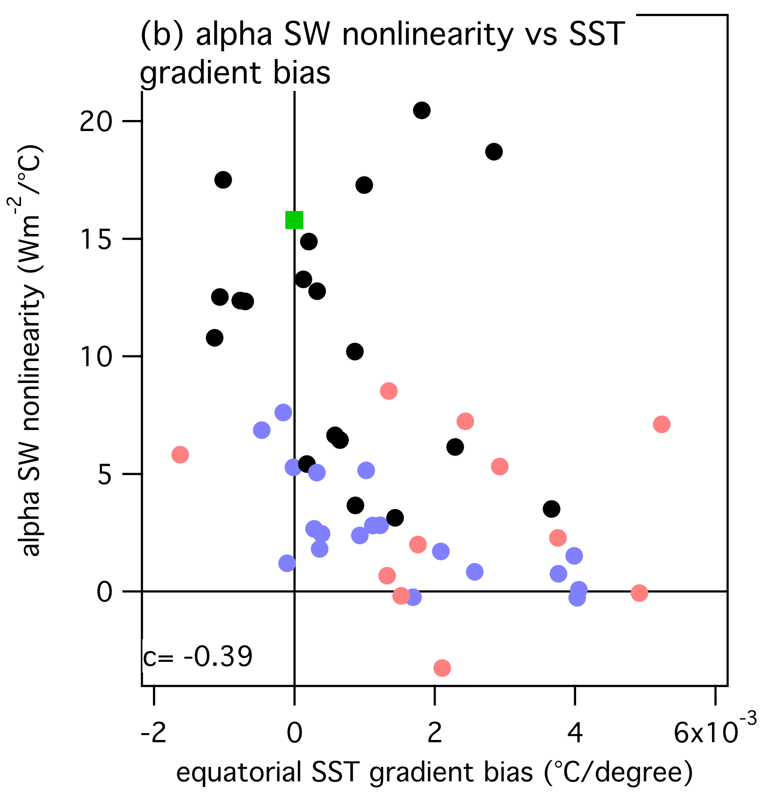

(b) alpha SW nonlinearity vs SST gradient bias
c= -0.39
alpha SW nonlinearity (Wm^-2 /°C)
equatorial SST gradient bias (°C/degree)
-2
0
2
4
6x10^-3
20
15
10
5
0

Figure 13

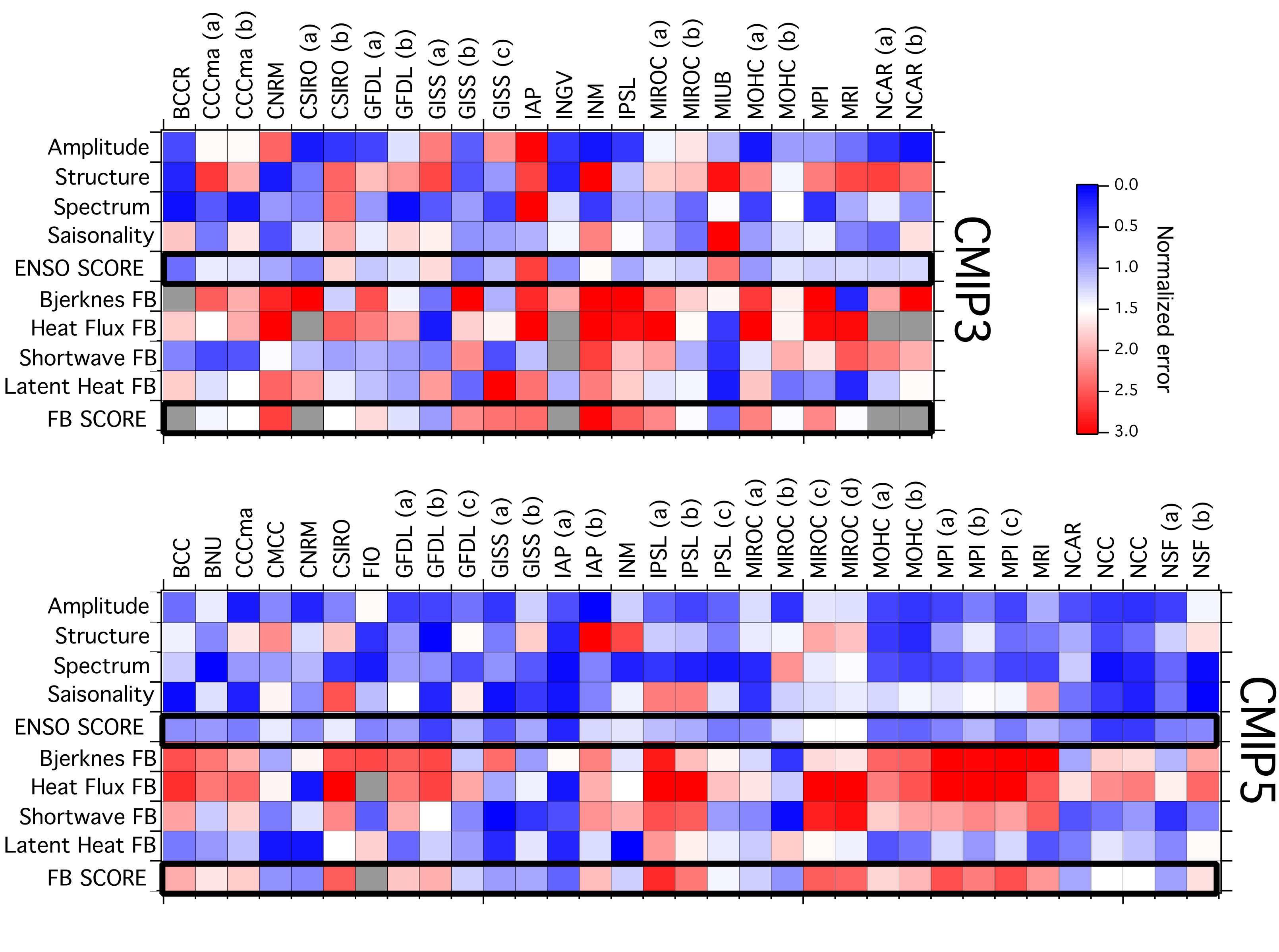
BCCR
CCCma (a)
CCCma (b)
CNRM
CSIRO (a)
CSIRO (b)
GFDL (a)
GFDL (b)
GISS (a)
GISS (b)
GISS (c)
IAP
INGV
INM
IPSL
MIROC (a)
MIROC (b)
MIUB
MOHC (a)
MOHC (b)
MPI
MRI
NCAR (a)
NCAR (b)
Amplitude
Structure
Spectrum
Saisonality
ENSO SCORE
Bjerknes FB
Heat Flux FB
Shortwave FB
Latent Heat FB
FB SCORE
CMIP3
0.0
0.5
1.0
1.5
2.0
2.5
3.0
Normalized error
BCC
BNU
CCCma
CMCC
CNRM
CSIRO
FIO
GFDL (a)
GFDL (b)
GFDL (c)
GISS (a)
GISS (b)
IAP (a)
IAP (b)
INM
IPSL (a)
IPSL (b)
IPSL (c)
MIROC (a)
MIROC (b)
MIROC (c)
MIROC (d)
MOHC (a)
MOHC (b)
MPI (a)
MPI (b)
MPI (c)
MRI
NCAR
NCC
NCC
NSF (a)
NSF (b)
Amplitude
Structure
Spectrum
Saisonality
ENSO SCORE
Bjerknes FB
Heat Flux FB
Shortwave FB
Latent Heat FB
FB SCORE
CMIP5

Figure 14

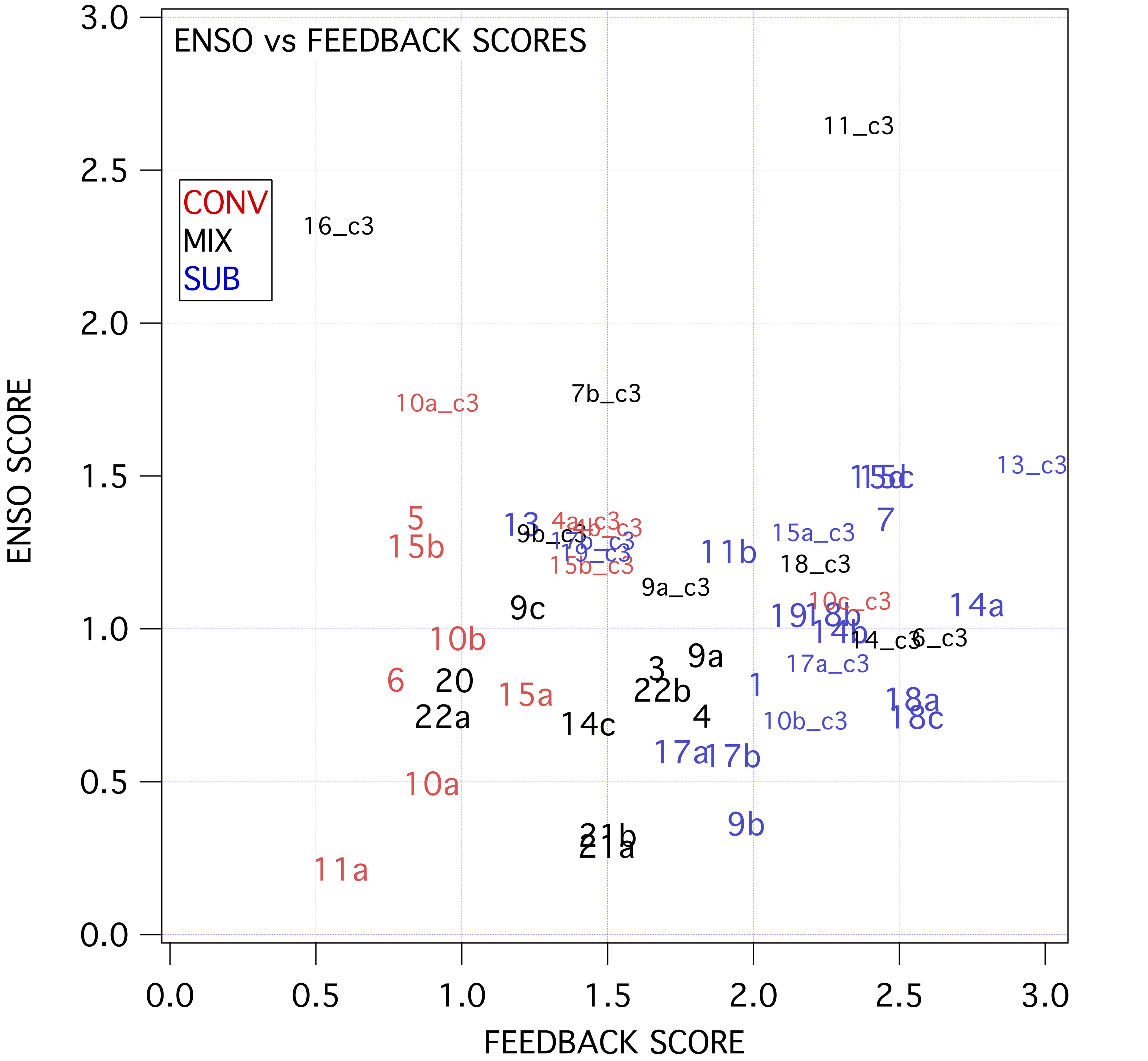
ENSO vs FEEDBACK SCORES
CONV
MIX
SUB
ENSO SCORE
FEEDBACK SCORE
0.0
0.5
1.0
1.5
2.0
2.5
3.0
11_c3
16_c3
10a_c3
7b_c3
13_c3
5
15b
9c
10b
6
20
22a
15a
14c
10a
11a
21b
21a
3
22b
9a
4
9a_c3
18_c3
15a_c3
11b
7
14a
17a_c3
10b_c3
17a
17b
9b
1
18a
18c